

# Stationary perturbation configurations in a composite system of stellar and coplanarly magnetized gaseous singular isothermal discs

Yu-Qing Lou<sup>1,2,3</sup> and Yue Zou<sup>1</sup>

<sup>1</sup>*Physics Department, The Tsinghua Center for Astrophysics, Tsinghua University, Beijing 100084, China*

<sup>2</sup>*Department of Astronomy and Astrophysics, The University of Chicago, 5640 Ellis Ave, Chicago, IL 60637, USA*

<sup>3</sup>*National Astronomical Observatories, Chinese Academy of Science, A20, Datun Road, Beijing 100012, China*

Accepted 2004... Received 2003...; in original form 2003

## ABSTRACT

We construct aligned and unaligned stationary perturbation configurations in a composite system of stellar and coplanarly magnetized gaseous singular isothermal discs (SIDs) coupled by gravity. This study extends recent analyses on (magnetized) SIDs of Shu et al., Lou and Lou & Shen. By this model, we intend to provide a conceptual framework to gain insights for multi-wavelength large-scale structural observations of disc galaxies. Both SIDs are approximated to be razor-thin and are in a self-consistent axisymmetric background equilibrium with power-law surface mass densities and flat rotation curves. The gaseous SID is embedded with a coplanar azimuthal magnetic field  $B_\theta(r)$  of a radial scaling  $r^{-1/2}$  that is not force-free. In comparison with SID problems studied earlier, there exist three possible classes of stationary solutions allowed by more dynamic freedoms. To identify physical solutions, we explore parameter space involving three dimensionless parameters: ratio  $\lambda$  of Alfvén speed to sound speed in the magnetized gaseous SID, ratio  $\beta$  for the square of the stellar velocity dispersion to the gas sound speed and ratio  $\delta$  of the surface mass densities of the two SIDs. For both aligned and unaligned spiral cases with azimuthal periodicities  $|m| \geq 2$ , one of the three solution branches is always physical, while the other two branches might become invalid when  $\beta$  exceeds certain critical values. For the onset criteria from an axisymmetric equilibrium to aligned secular bar-like instabilities, the corresponding  $\mathcal{T}/|\mathcal{W} - \mathcal{M}|$  ratio, which varies with  $\lambda$ ,  $\beta$  and  $\delta$ , may be considerably lower than the oft-quoted value of  $\mathcal{T}/|\mathcal{W}| \sim 0.14$ , where  $\mathcal{T}$  is the total kinetic energy,  $\mathcal{W}$  is the total gravitational potential energy and  $\mathcal{M}$  is the total magnetic energy. For unaligned spiral cases, we examine marginal instabilities for axisymmetric ( $|m| = 0$ ) and non-axisymmetric ( $|m| > 0$ ) disturbances. The resulting marginal stability curves differ from the previous ones. The case of a composite partial MSID system is also investigated to include the gravitational effect of an axisymmetric dark matter halo on the SID equilibrium. We further examine the phase relationship among the mass densities of the two SIDs and azimuthal magnetic field perturbation. Our exact global perturbation solutions and critical points are valuable for testing numerical magnetohydrodynamic codes. For galactic applications, our model analysis contains more realistic elements and offer useful insights for structures and dynamics of disc galaxies consisting of stars and magnetized gas.

**Key words:** ISM: general — galaxies: kinematics and dynamics — galaxies: spiral — galaxies: structure — MHD — waves.

## 1 INTRODUCTION

In galactic contexts, we venture to formulate a theoretical magnetohydrodynamic (MHD) disc problem to explore pos-

sible large-scale structures and dynamics of stationary MHD density waves in a composite system of stellar and magnetized interstellar medium (ISM) gas discs. The two gravitationally coupled discs are treated as ‘fluid’ and ‘mag-

netofluid' respectively and are both expediently approximated as razor-thin singular isothermal discs (SIDs) with the gaseous SID being embedded with a coplanar azimuthal magnetic field. For the gravitational effect of a massive axisymmetric dark matter halo, we prescribe a background composite system of two coupled partial SIDs (Syer & Tremaine 1996; Shu et al. 2000; Lou 2002; Lou & Shen 2003; Shen & Lou 2003). In our model analysis, we construct stationary aligned and unaligned logarithmic spiral MHD perturbation configurations in a composite system of two SIDs with flat rotation curves, and attempt to relate various morphologies of disc galaxies, including barred and lopsided, barred and normal spiral structures. For possible observational diagnostics, we derive phase relationships among perturbation patterns of the stellar surface mass density, the gas surface mass density and the azimuthal magnetic field.

This introduction serves two purposes. The first one is to provide a general background information relevant to the problem at hand and the second one is to give reasons of pursuing this MHD disc problem.

In a pioneering study of a composite system of stellar and gas discs coupled by gravity, Lin & Shu (1966, 1968) used a stellar distribution function and a gas fluid disc description to derive and analyze the local dispersion relation of galactic spiral density waves. Since then, there have been extensive theoretical studies on perturbation configurations and stability properties of a composite disc system, mainly in galactic contexts. Kato (1972) investigated oscillations and overstabilities of density waves using a formalism similar to that of Lin & Shu (1966, 1968). In a two-fluid formalism, Jog & Solomon (1984a, b) examined the growth of local axisymmetric perturbations in a composite disc system. Bertin & Romeo (1988) studied the influence of a gas disc on spiral modes in a two-fluid model framework. Vandervoort (1991a, b) studied the influence of interstellar gas on oscillations and stabilities of spheroidal galaxies. The two-fluid approach was also adopted in a stability study of a two-component disc system with finite disc thickness by Romeo (1992). The analysis for morphologies of disc galaxies was performed by Lowe et al. (1994). For the stability of a composite disc system, different effective  $Q_{eff}$  parameters (Safronov 1960; Toomre 1964) have been suggested using a two-fluid formalism by Elmegreen (1995) and Jog (1996). Recently, Lou & Fan (1998b) used the two-fluid formalism to study properties of open and tight-winding spiral density-wave modes in a composite disc system. Lou & Shen (2003) studied stationary global perturbation structures in a two-fluid system of SIDs and, instead of a redefinition of a different  $Q_{eff}$  parameter, Shen & Lou (2003) offered a more practical  $D$ -criterion for the axisymmetric instability in a composite SID system.

A rich class of disc problems involves stability properties of SIDs. There have been numerous studies on this subject since the pioneering work of Mestel (1963) (e.g. Zang 1976; Toomre 1977; Lemos, Kalnajs & Lynden-Bell 1991; Lynden-Bell & Lemos 1999; Goodman & Evans 1999; Chakrabarti, Laughlin & Shu 2003). Specifically, Syer & Tremaine (1996)

made an important breakthrough to derive semi-analytic solutions for stationary perturbation configurations in a class of SIDs. Shu et al. (2000) obtained stationary solutions for perturbation configurations in an isopedically magnetized SID with a flat rotation curve. Through numerical explorations, they interpreted these stationary aligned and unaligned logarithmic spiral configurations as onsets of bar-type and barred-spiral instabilities (see also Galli et al. 2001). Different from yet complementary to the analysis of Shu et al. (2000), Lou (2002) performed a coplanar MHD perturbation analysis in a single background SID embedded with an azimuthal magnetic field, from the perspective of stationary fast and slow MHD density waves (FMDWs and SMDWs; Fan & Lou 1996; Lou & Fan 1998a). Lou (2002) also derived a form of magnetic virial theorem for an MSID and suggested the ratio of rotation energy to the sum of gravitational and magnetic energies to be crucial for the onset of bar-like instability in an MSID system. In galactic contexts, it would be more realistic to consider large-scale structures and dynamics in a composite system of stellar and magnetized ISM discs. As a first step, Lou & Shen (2003) made a foray on this model problem, constructed stationary aligned and unaligned logarithmic spiral configurations in such a composite SID system and further examined axisymmetric instability properties (Shen & Lou 2003).

In disc galaxies, the ISM disc is magnetized with the magnetic energy density being comparable to the energy densities of thermal gas and of relativistic cosmic-ray gas (e.g. Lou & Fan 2003). Information of galactic magnetic fields can be estimated by synchrotron radio emissions from spiral galaxies. For such a magnetized composite system, MHD will play an indispensable role and reveal more realistic aspects of dynamic and diagnostic information. These important problems (Shu et al. 2000; Lou 2002; Lou & Shen 2003) are not only interesting by themselves, but also serve as necessary steps for establishing an even more realistic model. Motivated by this prospect (Lou & Fan 1998b; Lou 2002; Lou & Shen 2003), we construct here stationary perturbation configurations for aligned and unaligned logarithmic spiral cases in a composite system of a stellar SID and a coplanarly magnetized gaseous MSID, and discuss their stability properties.

We adopt a relatively simple formalism for a composite system involving fluid and magnetofluid discs coupled by gravity. We provide in Section 2 an MHD description for the coplanarly magnetized gaseous MSID, obtain conditions for background axisymmetric equilibrium state for both stellar SID and gaseous MSID, and derive linearized equations for coplanar perturbations. There exist aligned and unaligned classes of global MHD perturbation solutions; they are analyzed in Section 3 and Section 4, respectively. The exact solutions of stationary perturbations, their stability properties and their corresponding phase relationships among perturbation variables are examined and summarized in Section 5. Details are included in Appendices A–E.

## 2 FLUID-MAGNETOFLUID FORMALISM

It would be physically more precise to adopt a distribution function formalism in dealing with a stellar disc especially in terms of singularities and resonances (e.g. Lin & Shu 1966, 1968; Binney & Tremaine 1987). For the present purpose of modelling large-scale stationary perturbation structures and for mathematical simplicity (Lou & Shen 2003), it suffices to start with the fluid-magnetofluid formalism, including an MHD treatment for the gaseous MSID (Lou 2002; Lou & Fan 2003). In this section, we present the basic equations for the fluid-magnetofluid system consisting of a stellar SID and a gaseous MSID. For flat rotation curves, conditions on the background rotational equilibrium with axisymmetry can be derived. We then obtain the linearized equations for coplanar MHD perturbations in the composite MSID system.

### 2.1 Basic Nonlinear MHD Equations

The two SIDs, located at  $z = 0$ , are both approximated as infinitesimally thin. In our fluid-magnetofluid treatment, the two SIDs are coupled through mutual gravitational interaction. For large-scale stationary perturbations, diffusive processes such as viscosity, ambipolar diffusion and thermal diffusion etc. are ignored. For physical variables under consideration, we shall use superscript or subscript  $s$  to indicate an association with the stellar SID and superscript or subscript  $g$  to indicate an association with the gaseous MSID. In cylindrical coordinates  $(r, \theta, z)$ , the basic fluid-magnetofluid equations for a composite MSID system can be readily written out.

In the fluid approximation for a stellar SID, the mass conservation, the radial component of the momentum equation and the azimuthal component of the momentum equation are given below in order, namely

$$\frac{\partial \Sigma^s}{\partial t} + \frac{1}{r} \frac{\partial(r \Sigma^s u^s)}{\partial r} + \frac{1}{r^2} \frac{\partial(\Sigma^s j^s)}{\partial \theta} = 0, \quad (1)$$

$$\frac{\partial u^s}{\partial t} + u^s \frac{\partial u^s}{\partial r} + \frac{j^s}{r^2} \frac{\partial u^s}{\partial \theta} - \frac{j^{s2}}{r^3} = -\frac{1}{\Sigma^s} \frac{\partial \Pi^s}{\partial r} - \frac{\partial \phi}{\partial r}, \quad (2)$$

$$\frac{\partial j^s}{\partial t} + u^s \frac{\partial j^s}{\partial r} + \frac{j^s}{r^2} \frac{\partial j^s}{\partial \theta} = -\frac{1}{\Sigma^s} \frac{\partial \Pi^s}{\partial \theta} - \frac{\partial \phi}{\partial \theta}, \quad (3)$$

where  $u^s$  is the radial component of the stellar bulk velocity,  $j^s \equiv r v^s$  is the stellar specific angular momentum along the  $\hat{z}$  direction; and  $v^s$  is the azimuthal component of the stellar bulk velocity;  $\phi$  is the total gravitational potential,  $\Pi^s$  is the vertically integrated (effective) pressure (sometimes referred to as the two-dimensional pressure), and  $\Sigma^s$  is the vertically integrated stellar mass density (i.e. stellar surface mass density).

In the magnetofluid approximation for the gaseous MSID, the mass conservation, the radial component of the momentum equation and the azimuthal component of the momentum equation are given below in order, namely

$$\frac{\partial \Sigma^g}{\partial t} + \frac{1}{r} \frac{\partial(r \Sigma^g u^g)}{\partial r} + \frac{1}{r^2} \frac{\partial(\Sigma^g j^g)}{\partial \theta} = 0, \quad (4)$$

$$\frac{\partial u^g}{\partial t} + u^g \frac{\partial u^g}{\partial r} + \frac{j^g}{r^2} \frac{\partial u^g}{\partial \theta} - \frac{j^{g2}}{r^3} = -\frac{1}{\Sigma^g} \frac{\partial \Pi^g}{\partial r} - \frac{\partial \phi}{\partial r} - \frac{1}{\Sigma^g} \int \frac{dz B_\theta}{4\pi r} \left[ \frac{\partial(r B_\theta)}{\partial r} - \frac{\partial B_r}{\partial \theta} \right], \quad (5)$$

$$\frac{\partial j^g}{\partial t} + u^g \frac{\partial j^g}{\partial r} + \frac{j^g}{r^2} \frac{\partial j^g}{\partial \theta} = -\frac{1}{\Sigma^g} \frac{\partial \Pi^g}{\partial \theta} - \frac{\partial \phi}{\partial \theta} + \frac{1}{\Sigma^g} \int \frac{dz B_r}{4\pi} \left[ \frac{\partial(r B_\theta)}{\partial r} - \frac{\partial B_r}{\partial \theta} \right], \quad (6)$$

where  $u^g$  is the radial component of the gas bulk velocity,  $j^g \equiv r v^g$  is the gas specific angular momentum along the  $\hat{z}$  direction,  $v^g$  is the azimuthal component of the gas bulk velocity,  $\Pi^g$  is the vertically integrated gas pressure (sometimes referred to as the two-dimensional gas pressure),  $\Sigma^g$  is the vertically integrated gas mass density (i.e. gas surface mass density) and  $B_r$  and  $B_\theta$  are the radial and azimuthal components of magnetic field  $\mathbf{B}$ . The last two terms on the right-hand sides of equations (5) and (6) are the radial and azimuthal components of the Lorentz force due to the coplanar magnetic field. The coupling of the two sets of fluid and magnetofluid equations (1) – (3) and (4) – (6) is effected by the total gravitational potential  $\phi$  through the Poisson integral, namely

$$F\phi(r, \theta, t) = \oint d\psi \int_0^\infty \frac{-G(\Sigma^g + \Sigma^s)\zeta d\zeta}{[\zeta^2 + r^2 - 2\zeta r \cos(\psi - \theta)]^{1/2}}, \quad (7)$$

where  $F$  is a constant ratio with  $0 < F \leq 1$ ;  $F\phi$  is the gravitational potential from the stellar SID and gaseous MSID together, and the fraction  $(1 - F)\phi$  is attributed to an axisymmetric dark matter halo that is unresponsive to coplanar MHD perturbations in the composite MSID system (e.g. Shu et al. 2000).

The divergence-free condition for the coplanar magnetic field  $\mathbf{B} = (B_r, B_\theta, 0)$  is

$$\frac{\partial(r B_r)}{\partial r} + \frac{\partial B_\theta}{\partial \theta} = 0, \quad (8)$$

and the radial and azimuthal components of magnetic induction equation are

$$\frac{\partial B_r}{\partial t} = \frac{1}{r} \frac{\partial}{\partial \theta} (u^g B_\theta - v^g B_r), \quad (9)$$

$$\frac{\partial B_\theta}{\partial t} = -\frac{\partial}{\partial r} (u^g B_\theta - v^g B_r). \quad (10)$$

Equations (1) – (10) form the basis of our theoretical analysis.

### 2.2 Rotational MSID Equilibrium

For a flat rotation curve in a stellar SID, we write the corresponding angular rotation rate in the form of

$$\Omega_s(r) = a_s \frac{D_s}{r}, \quad (11)$$

where  $a_s$ , mimicking an ‘effective isothermal sound speed’, represents the velocity dispersion of the stellar SID and  $D_s$  is a dimensionless parameter for stellar SID rotation. We invoke the expedient polytropic approximation

$$\Pi_0^s = a_s^2 \Sigma_0^s \quad (12)$$

to relate the two-dimensional pressure and the surface mass density. The epicyclic frequency  $\kappa_s$  of the stellar disk is defined by

$$\kappa_s^2 \equiv \frac{2\Omega_s}{r} \frac{d}{dr}(r^2\Omega_s) = 2\Omega_s^2. \quad (13)$$

In parallel, we have the angular rotation rate of the gaseous MSID as

$$\Omega_g(r) = a_g \frac{D_g}{r}, \quad (14)$$

where  $a_g$  is the isothermal sound speed of the gaseous MSID and  $D_g$  is a dimensionless parameter for MSID rotation. The polytropic relation and the definition of the epicyclic frequency  $\kappa_g$  for the gaseous MSID are simply

$$\Pi_0^g = a_g^2 \Sigma_0^g, \quad (15)$$

$$\kappa_g^2 = 2\Omega_g^2. \quad (16)$$

To avoid the magnetic field winding dilemma in a rotating disc (e.g. Lou & Fan 1998a), the background coplanar magnetic field, which is not force-free, is taken to be purely azimuthal about the symmetry  $\hat{z}$ -axis:

$$B_\theta(r) = \mathcal{F} r^{-\frac{1}{2}}, \quad (17)$$

where  $\mathcal{F}$  is a constant (Lou 2002) proportional to the encircled magnetic flux within  $r$ , and

$$B_r = B_z = 0. \quad (18)$$

In galactic model applications, one needs to invoke a central bulge or other processes to avoid the divergence of  $B_\theta$  as  $r \rightarrow 0$ . From the radial momentum equations (2) and (5) in a rotational equilibrium and the fact that  $F\partial\phi/\partial r = 2\pi G(\Sigma_0^s + \Sigma_0^g)$  by Poisson integral (7), one derives the following expressions for the background surface mass densities, namely

$$\Sigma_0^s = F \frac{a_s^2(1 + D_s^2)}{2\pi G r} \frac{1}{(1 + \delta)}, \quad (19)$$

$$\Sigma_0^g = F \frac{a_g^2(1 + D_g^2) - C_A^2/2}{2\pi G r} \frac{\delta}{(1 + \delta)}, \quad (20)$$

where  $\delta \equiv \Sigma_0^g/\Sigma_0^s$  is the surface mass density ratio of the two coupled background SIDs and  $C_A$  is the Alfvén wave speed in the MSID defined by

$$C_A^2 \equiv \int dz B_\theta^2 / (4\pi \Sigma_0). \quad (21)$$

From equations (19) and (20), it then follows that

$$a_s^2(1 + D_s^2) = a_g^2(1 + D_g^2) - C_A^2/2. \quad (22)$$

Physically, condition (22) results from the basic fact that the same total gravitational force  $\partial\phi/\partial r$ , including the contribution from the dark matter halo, acts on both the stellar SID and magnetized gaseous SID, and is very useful in our analysis below. It should be noted that the rotation rates of the two SIDs are different in general (Lou & Shen 2003; Shen & Lou 2003). In dimensionless form, condition (22) can be written in the form of either

$$D_g^2 = \beta(1 + D_s^2) - 1 + \lambda^2/2 \quad (23)$$

or

$$D_s^2 = \frac{1}{\beta}(1 + D_g^2 - \lambda^2/2) - 1, \quad (24)$$

where parameter  $\beta \equiv a_s^2/a_g^2$  stands for the square of the ratio of the stellar velocity dispersion to the sound speed of the MSID, and parameter  $\lambda^2 \equiv C_A^2/a_g^2$  stands for the square of the ratio of the Alfvén speed to the sound speed in the MSID. In disc galaxies, the stellar velocity dispersion  $a_s$  is usually higher than the sound speed  $a_g$ , we naturally focus on the case of  $\beta \geq 1$  (e.g. Jog & Solomon 1984a, b; Bertin & Romeo 1988; Jog 1996; Elmegreen 1995; Lou & Fan 1998b; Lou & Shen 2003; Shen & Lou 2003). In this  $\beta \geq 1$  regime, it follows from condition (24) that

$$1 + D_s^2 \leq 1 + D_g^2 - \lambda^2/2 < 1 + D_g^2, \quad (25)$$

implying that for  $\beta \geq 1$ ,

$$D_s^2 < D_g^2. \quad (26)$$

Inequality (26) is very important to identify physically valid mathematical solutions of  $D_s^2$  for stationary MHD perturbations. For specified parameters  $\beta$  and  $\lambda^2$ ,  $D_s^2$  and  $D_g^2$  are related to each other linearly by condition (23). We emphasize that mathematical solutions of  $D_g^2$  and  $D_s^2$  become unphysical for either  $D_g^2 < 0$  or  $D_s^2 < 0$  or both. The key here is that by inequality (26), we only need to consider  $D_s^2 > 0$  because  $D_g^2$  must also be positive. In our analysis, we mainly use equation (23) to derive a cubic algebraic equation in terms of  $D_s^2$  and examine solution properties.

### 2.3 Perturbations in a Composite MSID System

For small coplanar MHD perturbations in a composite MSID system, basic nonlinear equations (1)–(10) can be linearized in a straightforward manner, namely

$$\frac{\partial \Sigma_1^s}{\partial t} + \frac{1}{r} \frac{\partial(r \Sigma_0^s u_1^s)}{\partial r} + \Omega_s \frac{\partial \Sigma_1^s}{\partial \theta} + \frac{\Sigma_0^s}{r^2} \frac{\partial j_1^s}{\partial \theta} = 0, \quad (27)$$

$$\frac{\partial u_1^s}{\partial t} + \Omega_s \frac{\partial u_1^s}{\partial \theta} - 2 \frac{\Omega_s j_1^s}{r} = - \frac{\partial}{\partial r} \left( a_s^2 \frac{\Sigma_1^s}{\Sigma_0^s} + \phi_1 \right), \quad (28)$$

$$\frac{\partial j_1^s}{\partial t} + \frac{r \kappa_s^2}{2\Omega_s} u_1^s + \Omega_s \frac{\partial j_1^s}{\partial \theta} = - \frac{\partial}{\partial \theta} \left( a_s^2 \frac{\Sigma_1^s}{\Sigma_0^s} + \phi_1 \right) \quad (29)$$

for coplanar hydrodynamic perturbations in a stellar SID, and

$$\frac{\partial \Sigma_1^g}{\partial t} + \frac{1}{r} \frac{\partial(r \Sigma_0^g u_1^g)}{\partial r} + \Omega_g \frac{\partial \Sigma_1^g}{\partial \theta} + \frac{\Sigma_0^g}{r^2} \frac{\partial j_1^g}{\partial \theta} = 0, \quad (30)$$

$$\begin{aligned} \frac{\partial u_1^g}{\partial t} + \Omega_g \frac{\partial u_1^g}{\partial \theta} - 2 \frac{\Omega_g j_1^g}{r} = & - \frac{\partial}{\partial r} \left( a_g^2 \frac{\Sigma_1^g}{\Sigma_0^g} + \phi_1 \right) \\ & - \frac{1}{\Sigma_0^g} \int \frac{dz B_\theta}{4\pi r} \left[ \frac{\partial(r b_\theta)}{\partial r} - \frac{\partial b_r}{\partial \theta} \right] \\ & + \frac{C_A^2 \Sigma_1^g}{2\Sigma_0^g r} - \frac{1}{\Sigma_0^g} \int \frac{dz b_\theta}{4\pi r} \frac{\partial(r B_\theta)}{\partial r}, \end{aligned} \quad (31)$$

$$\begin{aligned} \frac{\partial j_1^g}{\partial t} + \frac{r \kappa_g^2}{2\Omega_g} u_1^g + \Omega_g \frac{\partial j_1^g}{\partial \theta} = & - \frac{\partial}{\partial \theta} \left( a_g^2 \frac{\Sigma_1^g}{\Sigma_0^g} + \phi_1 \right) \\ & + \frac{1}{\Sigma_0^g} \int \frac{dz b_r}{4\pi} \frac{\partial(r B_\theta)}{\partial r} \end{aligned} \quad (32)$$

for coplanar MHD perturbations in a gaseous MSID,

$$F\phi_1 = -G \oint d\psi \int_0^\infty \frac{(\Sigma_1^g + \Sigma_1^s)\zeta d\zeta}{[\zeta^2 + r^2 - 2\zeta r \cos(\psi - \theta)]^{1/2}} \quad (33)$$

for the linearized Poisson integral, and

$$\frac{\partial(r b_r)}{\partial r} + \frac{\partial b_\theta}{\partial \theta} = 0, \quad (34)$$

$$\frac{\partial b_r}{\partial t} = \frac{1}{r} \frac{\partial}{\partial \theta} (u_1^g B_\theta - r \Omega_g b_r), \quad (35)$$

$$\frac{\partial b_\theta}{\partial t} = -\frac{\partial}{\partial r} (u_1^g B_\theta - r \Omega_g b_r) \quad (36)$$

for the linearized divergence-free condition and the linearized magnetic induction equation.

We do not consider vertical variations along  $z$  direction across the composite MSID system. With a harmonic  $\exp(i\omega t - im\theta)$  dependence for all perturbation variables, we introduce complex radial variations  $\mu_s(r)$ ,  $\mu_g(r)$ ,  $U_s(r)$ ,  $U_g(r)$ ,  $J_s(r)$ ,  $J_g(r)$ ,  $V(r)$ ,  $R(r)$  and  $Z(r)$  for  $\Sigma_1^s$ ,  $\Sigma_1^g$ ,  $u_1^s$ ,  $u_1^g$ ,  $j_1^s$ ,  $j_1^g$ ,  $\phi_1$ ,  $b_r$  and  $b_\theta$ , respectively. Thus, hydrodynamic equations (27)–(29) can be reduced to the form of

$$i(\omega - m\Omega_s)\mu_s + \frac{1}{r} \frac{\partial}{\partial r} (r \Sigma_0^s U_s) - \frac{im \Sigma_0^s}{r^2} J_s = 0, \quad (37)$$

$$i(\omega - m\Omega_s)U_s - \frac{2\Omega_s J_s}{r} = -\frac{\partial \Phi_s}{\partial r}, \quad (38)$$

$$i(\omega - m\Omega_s)J_s + \frac{r\kappa_s^2}{2\Omega_s} U_s = im\Phi_s \quad (39)$$

for the stellar SID, where  $\Phi_s \equiv a_s^2 \mu_s / \Sigma_0^s + V$ . Similarly, MHD equations (30)–(36) can be cast into the form of

$$i(\omega - m\Omega_g)\mu_g + \frac{1}{r} \frac{\partial}{\partial r} (r \Sigma_0^g U_g) - \frac{im \Sigma_0^g}{r^2} J_g = 0, \quad (40)$$

$$i(\omega - m\Omega_g)U_g - \frac{2\Omega_g J_g}{r} = -\frac{\partial \Phi_g}{\partial r} + \frac{C_A^2 \mu_g}{2\Sigma_0^g r} - \frac{1}{\Sigma_0^g} \int \frac{dz Z}{4\pi r} \frac{\partial(r B_\theta)}{\partial r} - \frac{1}{\Sigma_0^g} \int \frac{dz B_\theta}{4\pi r} \left[ \frac{\partial(r Z)}{\partial r} + imR \right], \quad (41)$$

$$i(\omega - m\Omega_g)J_g + \frac{r\kappa_g^2}{2\Omega_g} U_g = im\Phi_g + \frac{1}{\Sigma_0^g} \int \frac{dz R}{4\pi} \frac{\partial(r B_\theta)}{\partial r}, \quad (42)$$

where  $\Phi_g \equiv a_g^2 \mu_g / \Sigma_0^g + V$ ,

$$\frac{\partial(r R)}{\partial r} - imZ = 0, \quad (43)$$

$$i(\omega - m\Omega_g)R + \frac{im B_\theta}{r} U_g = 0, \quad (44)$$

$$i\omega Z = \frac{\partial}{\partial r} (r \Omega_g R) - \frac{\partial}{\partial r} (B_\theta U_g) \quad (45)$$

for coplanar MHD perturbations in the gaseous MSID. By setting angular frequency  $\omega = 0$  in coplanar MHD perturbation equations (33) and (37)–(45), we can construct global stationary MHD perturbation configurations in a composite system of MSIDs without invoking the WKB or tight-winding approximation and analyze their properties.

### 3 ALIGNED MHD CONFIGURATIONS

Coplanar perturbations in a composite MSID system can be classified as ‘aligned’ and ‘unaligned’ solutions (e.g. Kalnajs 1973; Shu et al. 2000; Lou 2002; Lou & Shen 2003). For aligned configurations, all streamlines and magnetic field lines are aligned in a composite MSID system. For unaligned spiral configurations, neighbouring streamlines shift relative to each other in a systematic manner (Kalnajs 1973); the same physical scenario holds true for neighbouring magnetic field lines (Lou & Fan 1998a).

In this section, we obtain the stationary dispersion relation for aligned coplanar MHD perturbations (both full and partial MSIDs) by perturbation equations (33) and (37)–(45) in the preceding section. The solution behaviours and the corresponding phase relationships are analyzed, mainly in the context of a full SID system (i.e.  $F = 1$ ). At the end of this section, we derive the MHD virial theorem for a composite MSID system and suggest the onset criterion for secular bar-like instabilities in a composite MSID system (Ostriker & Peebles 1973; Binney & Tremaine 1987; Shu et al. 2000; Lou 2002).

#### 3.1 Dispersion Relation for Aligned Perturbations

To construct stationary perturbation configurations of MSID that are aligned, we set  $\omega = 0$  in equations (37)–(45). Let us first set  $\partial/\partial t = 0$  or  $\omega = 0$  in equations (40)–(45) for coplanar MHD perturbations in the MSID to obtain

$$m\Omega_g \mu_g + \frac{1}{r} \frac{\partial}{\partial r} (r \Sigma_0^g i U_g) + \frac{m \Sigma_0^g}{r^2} J_g = 0, \quad (46)$$

$$m\Omega_g i U_g + \frac{2\Omega_g J_g}{r} = \frac{\partial \Phi_g}{\partial r} - \frac{C_A^2 \mu_g}{2\Sigma_0^g r} + \frac{C_A^2 m i U_g}{\Omega_g r^2} - \frac{C_A^2}{2r^{1/2}} \frac{\partial}{\partial r} \left( \frac{i U_g}{m\Omega_g r^{1/2}} \right) - \frac{C_A^2}{r^{1/2}} \frac{\partial}{\partial r} \left[ r \frac{\partial}{\partial r} \left( \frac{i U_g}{m\Omega_g r^{1/2}} \right) \right], \quad (47)$$

$$m\Omega_g J_g + \frac{r\kappa_g^2}{2\Omega_g} i U_g = -m\Phi_g + \frac{C_A^2 i U_g}{2\Omega_g r}, \quad (48)$$

$$iR = \frac{B_\theta i U_g}{\Omega_g r}, \quad (49)$$

$$Z = -\frac{i}{m} \frac{\partial(r R)}{\partial r}. \quad (50)$$

For aligned perturbations, we take the following potential-density pair (Shu et al. 2000; Lou 2002; Lou & Shen 2003)

$$\mu_s \propto 1/r, \quad (51)$$

$$\mu_g \propto 1/r, \quad (52)$$

$$V = -\frac{2\pi G r}{|m|} (\mu_s + \mu_g), \quad (53)$$

such that

$$\Phi_g \equiv a_g^2 \mu_g / \Sigma_0^g + V = \text{constant}. \quad (54)$$

For a constant  $iU_g$ , as will be shown presently, combinations of equations (46) and (48) and expressions (51)–(53) give

$$J_g = -\frac{\Omega_g r^2 \mu_g}{\Sigma_0^g}, \quad (55)$$

$$iU_g = m \frac{\Phi_g - \Omega_g^2 r^2 \mu_g / \Sigma_0^g}{C_A^2 / (2\Omega_g r) - \Omega_g r}. \quad (56)$$

As  $\Phi_g$  is constant by equation (54), it is clear that  $iU_g$  is another constant. Consequently, equations (55) and (47) give

$$\left[ m\Omega_g r - \frac{C_A^2 (m^2 - 1/2)}{m\Omega_g r} \right] iU_g - \frac{2\Omega_g^2 r^2 \mu_g}{\Sigma_0^g} + \frac{C_A^2 \mu_g}{2\Sigma_0^g} = 0. \quad (57)$$

Substitutions of expressions (53), (55) and (56) into equation (57) give a relation between  $\mu_g$  and  $\mu_s$ , namely

$$\left( \frac{a_g^2 - \Omega_g^2 r^2}{\Sigma_0^g r} - \frac{2\pi G}{|m|} + \frac{\mathcal{K}}{\mathcal{A}} \right) \mu_g = \frac{2\pi G}{|m|} \mu_s, \quad (58)$$

where two coefficients  $\mathcal{K}$  and  $\mathcal{A}$  are defined by

$$\mathcal{K} \equiv \frac{C_A^2 / 2 - 2\Omega_g^2 r^2}{\Sigma_0^g r} \quad (59)$$

and

$$\mathcal{A} \equiv \frac{m^2 \Omega_g^2 r^2 - C_A^2 (m^2 - 1/2)}{C_A^2 / 2 - \Omega_g^2 r^2}, \quad (60)$$

respectively. In parallel, we set  $\omega = 0$  in equations (37)–(39) for coplanar perturbations in the stellar disc and use relations (51)–(53) to obtain\* another relation between  $\mu_s$  and  $\mu_g$ , namely

$$\left( m^2 \frac{a_s^2 - \Omega_s^2 r^2}{\Sigma_0^s r} - 2\pi G|m| + \frac{2\Omega_s^2 r^2}{\Sigma_0^s r} \right) \mu_s = 2\pi G|m|\mu_g. \quad (61)$$

Combining equations (61) and (58), we derive the stationary dispersion relation

$$\begin{aligned} & \frac{r^2}{m^2} \times \frac{1}{m^2 \Omega_g^2 r^2 - C_A^2 (m^2 - 1/2)} \\ & \times \left[ (m^2 - 2)\Omega_s^2 r^2 + 2\pi G|m|\Sigma_0^s r - m^2 a_s^2 \right] \\ & \times \left\{ m^4 \Omega_g^4 - \left[ 2\Omega_g^2 + \left( \frac{C_A^2 + a_g^2}{r^2} - \frac{2\pi G \Sigma_0^g}{|m|r} \right) m^2 - \frac{2C_A^2}{r^2} \right] \right. \\ & \times m^2 \Omega_g^2 + \frac{m^2 C_A^2}{r^2} \left[ \left( \frac{a_g^2}{r^2} - \frac{2\pi G \Sigma_0^g}{|m|r} \right) \left( m^2 - \frac{1}{2} \right) - \frac{C_A^2}{4r^2} \right] \left. \right\} \\ & = 4\pi^2 G^2 \Sigma_0^s \Sigma_0^g \end{aligned} \quad (62)$$

for aligned coplanar MHD perturbations in a composite MSID system. In the absence of the mutual gravitational coupling between the MSID and the stellar SID, represented by the term on the right-hand side of equation (62), the left-hand side of equation (62) would give rise to two separate dispersion relations, one for the stellar SID and one for the gaseous MSID. The first one would be

$$(m^2 - 2)\Omega_s^2 r^2 + 2\pi G|m|\Sigma_0^s r - m^2 a_s^2 = 0, \quad (63)$$

\* In view of the exchange symmetry between the stellar and gas SIDs, relation (61) can also be obtained by simply setting  $C_A = 0$  in equation (58) and switching subscripts  $g$  and  $s$ .

which gives the stationary dispersion relation for aligned coplanar perturbations in a stellar SID alone, that is, a single SID without magnetic field. Substituting expressions (11) and (19) of  $\Omega_s$  and  $\Sigma_0^s$  (with  $F = 1$ ) into equation (63), we obtain

$$(|m| - 1)[D_s^2(|m| + 2) - |m|] = 0, \quad (64)$$

which is simply equation (26) of Shu et al. (2000).

The second factor in the curly braces on the left-hand side of equation (62) is

$$\begin{aligned} & m^4 \Omega_g^4 - \left[ 2\Omega_g^2 + \left( \frac{C_A^2 + a_g^2}{r^2} - \frac{2\pi G \Sigma_0^g}{|m|r} \right) m^2 - \frac{2C_A^2}{r^2} \right] m^2 \Omega_g^2 \\ & + \frac{m^2 C_A^2}{r^2} \left[ \left( \frac{a_g^2}{r^2} - \frac{2\pi G \Sigma_0^g}{|m|r} \right) \left( m^2 - \frac{1}{2} \right) - \frac{C_A^2}{4r^2} \right] = 0, \end{aligned} \quad (65)$$

which is the stationary dispersion relation for aligned coplanar MHD perturbations in the gaseous MSID alone, that is, a single MSID with a coplanar magnetic field. Equation (65) is simply equation (3.2.6) of Lou (2002).

By the above results, it is clear that equation (62) represents the dispersion relation for stationary MHD density waves in a composite MSID system. As both SID and MSID rotate, the stationarity of MHD density wave patterns in an inertial frame of reference imposes conditions on dimensionless rotation parameter  $D_s^2$  (or equivalently,  $D_g^2$ ). For the following analysis, we substitute expressions (11), (14), (19) and (20) into equation (62) to yield another form of stationary dispersion relation in a composite full or partial MSID system, namely

$$\begin{aligned} & \frac{1}{m^2} \times \frac{1}{m^2 D_g^2 - \lambda^2 (m^2 - 1/2)} \\ & \times \left[ (m^2 - 2)D_s^2 + F|m|\frac{1 + D_s^2}{1 + \delta} - m^2 \right] \times \left\{ m^4 D_g^4 - \left[ 2D_g^2 + \left( \lambda^2 + 1 - F\frac{1 + D_g^2 - \lambda^2/2}{|m|} \frac{\delta}{1 + \delta} \right) m^2 - 2\lambda^2 \right] \times m^2 D_g^2 \right. \\ & + \left[ \left( 1 - F\frac{1 + D_g^2 - \lambda^2/2}{|m|} \frac{\delta}{1 + \delta} \right) \left( m^2 - \frac{1}{2} \right) - \frac{\lambda^2}{4} \right] \\ & \times m^2 \lambda^2 \left. \right\} - F^2 \frac{(1 + D_s^2)(1 + D_g^2 - \lambda^2/2)\delta}{(1 + \delta)^2} = 0. \end{aligned} \quad (66)$$

A substitution of expression (23) for  $D_g^2$  into (66) gives a cubic algebraic equation in terms of  $D_s^2$ . Or equivalently, a substitution of expression (24) for  $D_s^2$  into (66) would yield a cubic algebraic equation in terms of  $D_g^2$ . As noted earlier, we focus on the cubic equation of  $D_s^2$  to identify physical solutions of  $D_s^2 \geq 0$ , because  $D_s^2 < D_g^2$  as a result of  $a_s^2 > a_g^2$  in typical disc galaxies.

For a later examination of spatial phase relationship between azimuthal magnetic field perturbation  $b_\theta$  and the surface mass density perturbation  $\Sigma_1^g$  of the gaseous MSID, we combine equations (49) and (50) to obtain

$$Z = -\frac{iU_g B_\theta}{2m\Omega_g r}, \quad (67)$$

relating the  $\theta$ -component of the magnetic field perturbation  $Z$  and the radial gas flow speed perturbation  $iU_g$ . Using

equations (57) and (67), one can eliminate  $iU_g$  to obtain

$$Z = -\frac{B_\theta \mu_g}{2\Sigma_0^g} \frac{(2\Omega_g^2 r^2 - C_A^2/2)}{[m^2 \Omega_g^2 r^2 - C_A^2(m^2 - 1/2)]}, \quad (68)$$

that can be further reduced to

$$\frac{\mu_g}{Z} = -\frac{2\Sigma_0^g}{B_\theta} \frac{[m^2 D_g^2 - \lambda^2(m^2 - 1/2)]}{2D_g^2 - \lambda^2/2}. \quad (69)$$

For real  $\mu_g/Z$ , the sign of the right-hand side of the equation (69) will determine the phase relationship between the azimuthal magnetic field perturbation  $b_\theta$  and the gas surface mass density perturbation  $\Sigma_1^g$  in the gaseous MSID. That is,  $b_\theta$  and  $\Sigma_1^g$  are in and out of phase for a positive and negative right-hand side of the equation (69), respectively.

### 3.2 Axisymmetric Disturbances with $|m| = 0$

For aligned axisymmetric disturbances with  $|m| = 0$ , it would be inappropriate to directly use relation (62) or (66). One should carefully examine equations (37)–(45) with  $\omega = m = 0$ . With  $U_g = U_s = R = 0$ , equations (37), (39), (40), (42), (43) and (45) can be satisfied, and equation (44) is identically zero. By choosing  $Z \propto r^{-1/2}$ ,  $\mu_g \propto r^{-1}$ ,  $\mu_s \propto r^{-1}$ ,  $J_g \propto r$ ,  $J_s \propto r$ ,  $V \propto \ln r$ ,  $\Phi_g \propto \ln r + \text{constant}$  and  $\Phi_s \propto \ln r + \text{constant}$ , the two remaining equations (38) and (41) are consistent with a rescaling of the axisymmetric background. In the present context, this rescaling is somewhat trivial. We turn to cases of  $|m| \geq 1$  below.

### 3.3 Nonaxisymmetric Disturbances with $|m| \geq 1$

#### 3.3.1 Behaviours of $D_s^2$ solutions

We first come to the aligned case of  $|m| = 1$ . For a full composite MSID system with  $F = 1$ , it is easy to verify that equation (66) can be satisfied for arbitrary  $D_s^2$ . This is quite similar to cases of a single SID studied by Shu et al. (2000), of a single MSID studied by Lou (2002) and a composite SID system studied by Lou & Shen (2003). However, we note that for a single partial MSID (Lou 2002) and for a composite system of two coupled partial SIDs (Lou & Shen 2003), such stationary aligned eccentric  $|m| = 1$  perturbations are not allowed for arbitrary  $D_s^2$ . Likewise, in our case of a composite partial MSID system with  $F < 1$ , it is easy to see that equation (66) can no longer be satisfied for arbitrary  $D_s^2$  by simply setting  $|m| = 1$ .

In the following, we analyze cases of  $|m| \geq 2$  and focus on the special case of  $F = 1$  for a full composite MSID system. As mentioned earlier, we work in the parameter regime of  $\beta \geq 1$  with a typical disc galaxy in mind. By an extensive numerical exploration of aligned cases from  $|m| = 2$  to  $|m| = 5$ , we note empirically that cases of  $|m| > 2$  are fairly similar to the case of  $|m| = 2$ . For this reason, we shall mainly consider the case of  $|m| = 2$ . As noted earlier, we can substitute expression (23) for  $D_g^2$  into equation (66) to derive a cubic algebraic equation of  $y \equiv D_s^2$  as

$$\mathcal{A} + \mathcal{B}y + \mathcal{C}y^2 + \mathcal{D}y^3 = 0, \quad (70)$$

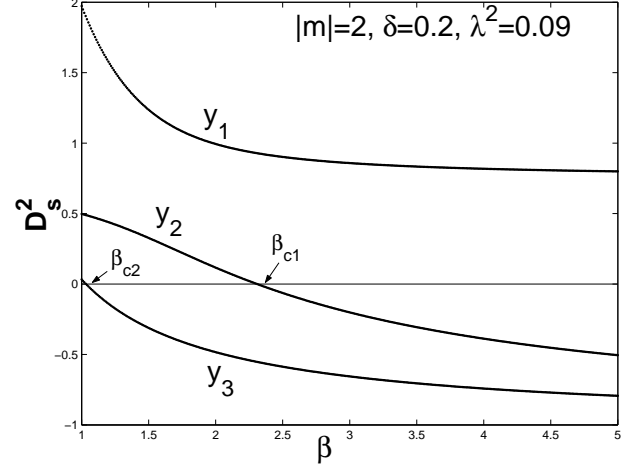


**Figure 1.** Three solution curves of  $D_s^2$  versus  $\beta$  for the aligned case with  $|m| = 2$ ,  $\delta = 0.2$  and  $\lambda^2 = 0.09$ .

where  $|m| = 2$  and  $F = 1$ , and the four coefficients  $\mathcal{A}$ ,  $\mathcal{B}$ ,  $\mathcal{C}$  and  $\mathcal{D}$  are explicitly defined by

$$\mathcal{A} \equiv 24 - 32\beta - 3\lambda^4 + 12\lambda^2\delta + 48\delta - 80\beta\delta - 6\beta\lambda^2\delta + 8\beta^2 + 6\lambda^2 + 32\beta^2\delta - 6\lambda^4\delta,$$

$$\mathcal{B} \equiv -12\lambda^2 - 3\beta\lambda^2\delta - 48 + 32\beta + 48\beta^2\delta - 40\beta\delta - 24\delta + 6\lambda^4 - 6\lambda^2\delta + 3\lambda^4\delta,$$

$$\mathcal{C} \equiv 3\beta\lambda^2\delta + 40\beta\delta + 64\beta - 24\beta^2$$

and

$$\mathcal{D} \equiv -16\beta^2\delta - 16\beta^2,$$

respectively.

Formally, three mathematical solutions for  $y \equiv D_s^2$  can be written out analytically from cubic equation (70) or from the more general cubic dispersion relation (66) with  $|m| > 2$  and  $F < 1$ , although the solution expressions are fairly involved (see Appendix C for details). Practically, we explore numerically various parameter regimes for the three  $D_s^2$  solutions. For specified values of parameters  $\delta$  and  $\lambda^2$ , we show three mathematical solutions  $y \equiv D_s^2$  versus  $\beta$  in Figs. 1–3.

For typical parameters, the three solution branches of  $D_s^2$  do not intersect with each other. For the convenience of discussion, we use  $y_1$ ,  $y_2$  and  $y_3$  to denote the upper, middle and lower solution branches, respectively. Generally speaking, the upper two solution branches,  $y_1$  and  $y_2$ , are qualitatively similar to those in a composite unmagnetized SID system (Lou & Shen 2003), that is,  $y_1$  branch remains always positive, while  $y_2$  decreases monotonically with increasing  $\beta$  and becomes negative when  $\beta$  exceeds a certain critical value  $\beta_{c1}$ . As expected for small  $\lambda^2$  (i.e. weak magnetic field; see Fig. 1),  $y_1$  and  $y_2$  respectively obey the limits of those in a composite SIDs without magnetic field [see equations (54) and (55) of Lou & Shen (2003)], showing that as  $\lambda^2 \rightarrow 0$ ,  $y_1$  and  $y_2$  consistently approach the upper and lower branches respectively of Lou & Shen (2003). One novel feature is the lowest solution branch  $y_3$  owing to the presence of magnetic

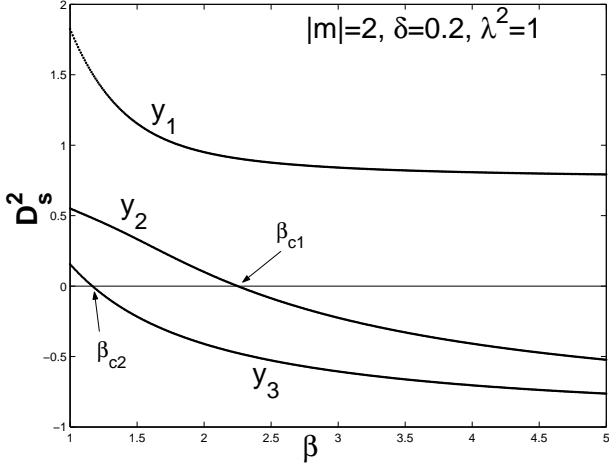


**Figure 2.** Three solution curves of  $D_s^2$  versus  $\beta$  for the aligned case with  $|m| = 2$ ,  $\delta = 0.2$  and  $\lambda^2 = 1$ .

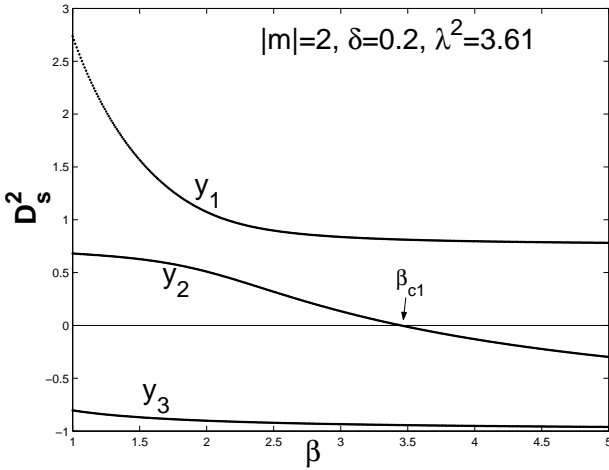


**Figure 3.** Three solution curves of  $D_s^2$  versus  $\beta$  for the aligned case with  $|m| = 2$ ,  $\delta = 0.2$  and  $\lambda^2 = 3.61$ .

field. In most cases,  $y_3$  is negative when  $\beta$  varies from 1 to  $+\infty$ , but for some special parameters,  $y_3$  may become positive when  $\beta$  becomes smaller than a critical value  $\beta_{c2}$ . Analytical expressions of  $\beta_{c1}$  and  $\beta_{c2}$  for the case of  $|m| = 2$  can be derived from a quadratic equation and are given by the following pair

$$\beta_{c1} \equiv \frac{1}{8 + 32\delta} [40\delta + 16 + 3\lambda^2\delta + (64\delta^2 + 128\delta - 144\lambda^2\delta^2 + 64 - 192\lambda^2\delta + 201\lambda^4\delta^2 + 24\lambda^4 + 144\lambda^4\delta - 48\lambda^2)^{1/2}] \quad (71)$$

and

$$\beta_{c2} \equiv \frac{1}{8 + 32\delta} [40\delta + 16 + 3\lambda^2\delta - (64\delta^2 + 128\delta - 144\lambda^2\delta^2 + 64 - 192\lambda^2\delta + 201\lambda^4\delta^2 + 24\lambda^4 + 144\lambda^4\delta - 48\lambda^2)^{1/2}] \quad (72)$$

respectively, where  $\beta_{c1}$  remains always larger than  $\beta_{c2}$ . We note the following. First, there is no essential mathematical difficulty of obtaining more general forms of  $\beta_{c1}$  and  $\beta_{c2}$  for

arbitrary  $|m|$  values with  $0 < F < 1$ . Secondly, by setting  $\lambda^2 = 0$  in expression (71) for  $\beta_{c1}$ , we obtain

$$\beta_{c1} = \frac{3}{2} \left( 1 + \frac{1}{4\delta + 1} \right), \quad (73)$$

consistent with the case of  $|m| = 2$  in expression (56) for  $\beta_c$  by Lou & Shen (2003). Finally, while  $\beta_{c2}$  is real in many cases [i.e. a positive determinant in both expressions (71) and (72)],  $\beta_{c2}$  may be too small to be discernible in the parameter regime of  $\beta \geq 1$ . For some special parameters specified,  $\beta_{c2}$  becomes noticeable. For example, in Fig. 2 with  $\delta = 0.2$  and  $\lambda^2 = 1$ , we have  $\beta_{c2} = 1.1667 > 1$  according to expression (72). In this case, for  $\beta$  smaller than 1.1667 (still quite restrictive), there exist three positive solutions of  $D_s^2$ . For  $\beta_{c2} < \beta < \beta_{c1}$ , the upper two branches  $y_1$  and  $y_2$  are positive, corresponding to two possible stationary perturbation modes. When  $\beta$  exceeds  $\beta_{c1}$ , only  $y_1$  remains positive, corresponding to one possible stationary perturbation mode. For the usual case of  $\beta_{c2} < 1$ , there are at most two possible stationary modes when  $\beta \rightarrow 1$  (see Fig. 3).

### 3.3.2 Phase relationships among perturbation variables

We now examine phase relationships among the azimuthal magnetic field and the surface mass density perturbations, because they may provide clues for magnetized spiral galaxies through optical and synchrotron radio observations (e.g. Mathewson et al. 1972; Beck & Hoernes 1996; Fan & Lou 1996; Lou & Fan 1998a, 2002, 2003; Frick et al. 2000, 2001; Lou 2002; Lou et al. 2002). For the phase relationship between the two surface mass density perturbations  $\mu_g$  and  $\mu_s$ , a combination of expressions (11), (19) and equation (61) gives

$$\frac{\mu_g}{\mu_s} = -1 - \frac{[y(m^2 - 2) - m^2](1 + \delta)}{|m|(y + 1)} \quad (74)$$

where  $y \equiv D_s^2$ . A substitution of expression (74) into equation (70) leads to a cubic algebraic equation of  $\mu_g/\mu_s$ . We show different curves of  $\mu_g/\mu_s$  versus  $\beta$  in Figs. 4 and 5 by specifying different values of  $\delta$  and  $\lambda^2$ .

In parallel, we examine the phase relationship between the azimuthal magnetic field perturbation  $b_\theta$  and the surface mass density perturbation  $\Sigma_1^g$  in the gaseous MSID. By equation (69), we introduce a dimensionless  $q$  parameter

$$q \equiv -\frac{[m^2 D_g^2 - \lambda^2(m^2 - 1/2)]}{2D_g^2 - \lambda^2/2}, \quad (75)$$

whose sign determines the phase relationship between  $Z$  and  $\mu_g$ . Using equation (75), we may express  $D_g^2$  as a function of  $q$ , namely

$$D_g^2 = \frac{\lambda^2(q + 2m^2 - 1)}{4q + 2m^2}. \quad (76)$$

A combination of equation (66) and expression (24) gives a cubic algebraic equation of  $D_g^2$ ; and a substitution of expression (76) into the resulting cubic equation of  $D_g^2$  leads to a cubic equation in terms of  $q$  (with  $|m| = 2$ ). We present different curves of  $q$  versus  $\beta$  for different values of  $\delta$  and  $\lambda^2$  in Figs. 6–7.



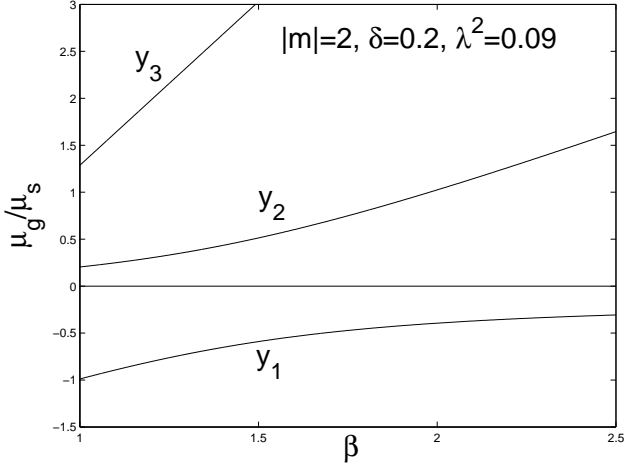


**Figure 4.** Curves of  $\mu_g/\mu_s$  versus  $\beta$  for the aligned  $|m| = 2$  case with  $\delta = 0.2$  and  $\lambda^2 = 0.09$ .

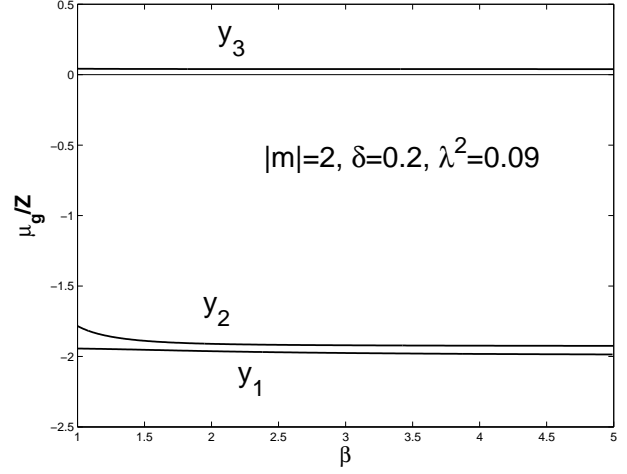


**Figure 6.** Curves of  $\mu_g/Z$  versus  $\beta$  for the aligned  $|m| = 2$  case with  $\delta = 0.2$  and  $\lambda^2 = 0.09$ .

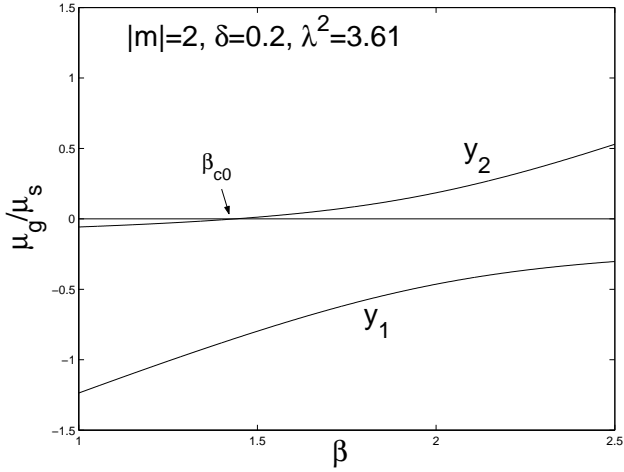


**Figure 5.** Curves of  $\mu_g/\mu_s$  versus  $\beta$  for the aligned  $|m| = 2$  case with  $\delta = 0.2$  and  $\lambda^2 = 3.61$ . The uppermost branch related to  $y_3$  is only discernible for  $\beta < 1$  and is not shown here. Specifically, this is caused by a negative  $y_3$  when  $\beta > 1$  (see Fig. 3).

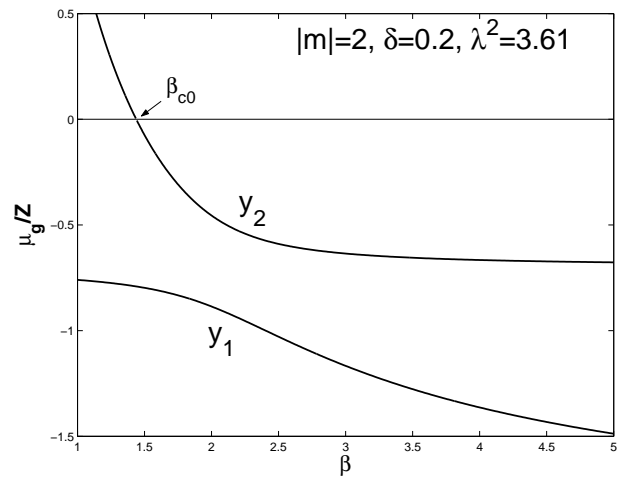


**Figure 7.** Curves of  $\mu_g/Z$  versus  $\beta$  for the aligned  $|m| = 2$  case with  $\delta = 0.2$  and  $\lambda^2 = 3.61$ . The uppermost branch related to  $y_3$  appears somewhat flat at about 44 and is not shown here.

From expressions (74) and (75), one can show that both larger  $\mu_g/\mu_s$  and  $\mu_g/Z$  correspond to smaller  $y$ . The lowest branches of  $\mu_g/\mu_s$  or  $\mu_g/Z$  are then related to the uppermost  $y_1$ ; the middle branches of  $\mu_g/\mu_s$  or  $\mu_g/Z$  are related to the middle  $y_2$ ; and the uppermost branches of  $\mu_g/\mu_s$  or  $\mu_g/Z$  are related to the lowest  $y_3$  as shown in Figs. 4–7.

Several interesting features are noted here for these curves. First, when  $\lambda^2$  is small (see Fig. 4), the lowest and middle branches of  $\mu_g/\mu_s$  respectively follow those in a composite SID system without magnetic fields [see equations (58) and (59) of Lou & Shen (2003)], showing consistently that as  $\lambda^2 \rightarrow 0$ , the middle and lowest branches of  $\mu_g/\mu_s$  correspond to the lower and upper branches of Lou & Shen (2003), respectively.

Secondly,  $\mu_g/\mu_s$  and  $\mu_g/Z$  of each solution branch of  $y$  bear definite signs in most cases. For the case of  $\delta = 0.2$  and  $\lambda^2 = 0.09$  as shown in Figs. 1, 4 and 6, the stationary perturbation mode of  $y_1$  branch has a phase relationship

between the surface mass density of the two SIDs (i.e.  $\mu_g/\mu_s$ ) and a phase relationship between the surface mass density of the MSID and the azimuthal magnetic field (i.e.  $\mu_g/Z$ ) being both always out of phase. In most cases, the stationary perturbation mode of  $y_2$  branch has a  $\mu_g/\mu_s$  being in phase (see Fig. 4) and a  $\mu_g/Z$  being out of phase (see Fig. 6). The stationary perturbation mode of  $y_3$  branch has  $\mu_g/\mu_s$  and  $\mu_g/Z$  being both always in phase (see Figs. 4 and 6).

Thirdly, for the stationary perturbation mode of  $y_2$  branch, both  $\mu_g/\mu_s$  and  $\mu_g/Z$  have a common zero point at  $\beta_{c0}$  that increases with increasing  $\lambda^2$ . For a sufficiently large  $\lambda^2$  (e.g.  $\lambda^2 = 3.61$ ),  $\beta_{c0}$  becomes greater than 1. Thus,  $\mu_g/\mu_s$  and  $\mu_g/Z$  may become zero or even carry opposite signs (see Figs. 5 and 7). Our analysis show that the middle  $y_2$  branch for  $\mu_g/\mu_s$  and  $\mu_g/Z$  has a common root at

$$\beta_{c0} = \frac{(6 + 3\delta)\lambda^2 + 8\delta + 16}{24(1 + \delta)}. \quad (77)$$

For a fixed  $\delta$ ,  $\beta_{c0}$  increases with increasing  $\lambda^2$ . Specifically

for  $\delta = 0.2$  and  $\lambda^2 = 0.09$  in expression (77), we have  $\beta_{c0} = 0.6317$  smaller than 1. Therefore, the middle  $y_2$  branch remains always positive (see Fig. 4). On the other hand, for  $\lambda^2 = 3.61$  in expression (77), we have  $\beta_{c0} = 1.4384$  larger than 1 (see Fig. 5).

It is not surprising that the middle  $y_2$  branch of  $\mu_g/\mu_s$  and  $\mu_g/Z$  has a common root as result of  $\mu_g = 0$ . The special  $\mu_g = 0$  case may be a possible situation in our model. By equation (55), it follows that  $J_g$  vanishes. As  $\mu_s$  and  $Z$  do not vanish, we see that  $V$ ,  $\Phi_g$  and consequently  $U_g$  do not vanish by expressions (53), (54) and (56).

Finally, our analysis show that the uppermost branch of  $\mu_g/\mu_s$  and  $\mu_g/Z$  corresponding to the  $y_3$  branch has a root at  $\beta = 0$ . It follows that  $y_3$  remains always positive.

### 3.4 Secular Barlike Instabilities

For the onset of aligned secular barlike instabilities in a composite MSID system, we here derive the MHD virial theorem for a composite MSID system (either full or partial) from the background radial equilibrium conditions (2) and (5)

$$-\Sigma_0^s r \Omega_s^2 = -\frac{d}{dr}(a_s^2 \Sigma_0^s) - \Sigma_0^s \frac{d\phi_0}{dr} \quad (78)$$

and

$$-\Sigma_0^g r \Omega_g^2 = -\frac{d}{dr}(a_g^2 \Sigma_0^g) - \Sigma_0^g \frac{d\phi_0}{dr} - \Sigma_0^g \frac{C_A^2}{2r}. \quad (79)$$

Adding equations (78) and (79), we readily obtain

$$(\Sigma_0^s \Omega_s^2 + \Sigma_0^g \Omega_g^2) r = \frac{d}{dr}(a_s^2 \Sigma_0^s + a_g^2 \Sigma_0^g) + (\Sigma_0^s + \Sigma_0^g) \frac{d\phi_0}{dr} + \Sigma_0^g \frac{C_A^2}{2r}. \quad (80)$$

Multiplying equation (80) by  $2\pi r^2 dr$  and integrating from 0 to a finite radius  $R$ , that is allowed to approach infinity eventually, we have the following MHD virial theorem.

$$2(\mathcal{T} + \mathcal{U}) + \mathcal{W} - \mathcal{M} = 2\pi R^2 [a_s^2 \Sigma_0^s(R) + a_g^2 \Sigma_0^g(R)] \quad (81)$$

within radius  $R$ , where

$$\mathcal{T} \equiv \int_0^R \frac{1}{2} \Sigma_0^s (r \Omega_s)^2 2\pi r dr + \int_0^R \frac{1}{2} \Sigma_0^g (r \Omega_g)^2 2\pi r dr \quad (82)$$

is the total rotational kinetic energy of the two SIDs,

$$\mathcal{W} \equiv - \int_0^R r (\Sigma_0^s + \Sigma_0^g) \frac{d\phi_0}{dr} 2\pi r dr \quad (83)$$

is the gravitational energy in the composite MSID system,

$$\mathcal{U} \equiv \int_0^R (a_s^2 \Sigma_0^s + a_g^2 \Sigma_0^g) 2\pi r dr \quad (84)$$

is the sum of stellar and gas internal energies and

$$\mathcal{M} \equiv \int_0^R \Sigma_0^g \frac{C_A^2}{2r} 2\pi r^2 dr \quad (85)$$

is the magnetic energy contained in the gaseous MSID component.

For a full composite system with  $F = 1$ , we combine relations (11), (14), (19) and (20) with expressions (82)–(85) to obtain

$$\begin{aligned} \mathcal{T} &= \int_0^R \frac{1}{2} \Sigma_0^s (r \Omega_s)^2 2\pi r dr + \int_0^R \frac{1}{2} \Sigma_0^g (r \Omega_g)^2 2\pi r dr \\ &= a_s^4 (D_s^2 + 1) \frac{D_s^2 + [D_s^2 + 1 + \lambda^2/(2\beta) - 1/\beta]\delta}{2G(1 + \delta)} R, \end{aligned} \quad (86)$$

$$\mathcal{W} = - \int_0^R r (\Sigma_0^s + \Sigma_0^g) \frac{d\phi_0}{dr} 2\pi r dr = - \frac{a_s^4 (D_s^2 + 1)^2}{G} R, \quad (87)$$

$$\mathcal{M} = \int_0^R \Sigma_0^g \frac{C_A^2}{2r} 2\pi r^2 dr = \frac{\lambda^2 a_s^4 (1 + D_s^2) \delta}{2G\beta(1 + \delta)} R. \quad (88)$$

Based on early numerical simulations (Hohl 1971; Miller et al. 1970), it was known that a thin self-gravitating disc in rotation may rapidly evolve into bar configurations (e.g. Binney & Tremaine 1987). Ostriker & Peebles (1973) suggested an approximate criterion  $\mathcal{T}/|\mathcal{W}| \leq 0.14 \pm 0.02$ , necessary but not sufficient, for stability against bar-type instabilities, on the basis of their  $N$ -body numerical explorations involving 300 particles. In the presence of a coplanar azimuthal magnetic field with a radial scaling of  $\propto r^{-1/2}$ , Lou (2002) proposed that the ratio  $\mathcal{T}/|\mathcal{W} - \mathcal{M}|$  may play the role of  $\mathcal{T}/|\mathcal{W}|$  in an unmagnetized SID to determine the onset of instability in a single MSID. By the above analogy and a natural extension, we use  $\mathcal{T}/|\mathcal{W} - \mathcal{M}|$  instead of  $\mathcal{T}/|\mathcal{W}|$  to examine the onset criterion of instability in a full composite MSID system in the presence of coplanar non-axisymmetric aligned MHD perturbations. Using expressions (86), (87) and (88), we arrive at

$$\begin{aligned} \frac{\mathcal{T}}{|\mathcal{W} - \mathcal{M}|} &= \frac{-2\delta + 2\delta\beta + \delta\lambda^2 + (2\delta\beta + 2\beta)D_s^2}{2\delta\lambda^2 + 4\beta + 4\delta\beta + (4\beta + 4\delta\beta)D_s^2} \\ &= \frac{1}{2} - \frac{\beta + \delta}{\delta\lambda^2 + 2\beta(1 + \delta)(D_s^2 + 1)}, \end{aligned} \quad (89)$$

indicating that the value of  $\mathcal{T}/|\mathcal{W} - \mathcal{M}|$  falls between 0 and 1/2 as in the unmagnetized case (Lou & Shen 2003) and increases with increasing  $D_s^2$ . Therefore in a composite MSID system, the three possible values of  $D_s^2$  correspond to three different values of  $\mathcal{T}/|\mathcal{W} - \mathcal{M}|$  ratio; and larger values of  $D_s^2$  correspond to higher  $\mathcal{T}/|\mathcal{W} - \mathcal{M}|$  ratios.

We here examine a few cases to illustrate the utility of our proposed onset criterion for instability. First, we set  $|m| = 2$ ,  $\delta = 0.2$ ,  $\beta = 1$  and  $\lambda^2 = 1$ . From equation (70), one obtains three  $D_s^2$  solutions  $D_s^2 = 1.8246$ ,  $D_s^2 = 0.5513$  and  $D_s^2 = 0.1553$ . Insertions of these three values of  $D_s^2$  into expression (89) would give  $\mathcal{T}/|\mathcal{W} - \mathcal{M}| = 0.3281$ ,  $\mathcal{T}/|\mathcal{W} - \mathcal{M}| = 0.1941$  and  $\mathcal{T}/|\mathcal{W} - \mathcal{M}| = 0.0963$ , respectively. As another example, we set  $|m| = 2$ ,  $\delta = 0.2$ ,  $\beta = 2$  and  $\lambda^2 = 1$ . From equation (70), we have  $D_s^2 = 0.9508$ ,  $D_s^2 = 0.1001$  and  $D_s^2 = -0.4103$ ; the third branch of solution should be ignored as  $D_s^2 < 0$ . The corresponding values of  $\mathcal{T}/|\mathcal{W} - \mathcal{M}|$  for the first two  $D_s^2$  solutions are  $\mathcal{T}/|\mathcal{W} - \mathcal{M}| = 0.2700$  and  $\mathcal{T}/|\mathcal{W} - \mathcal{M}| = 0.0986$ , respectively.

From these numerical estimates, it is clear that the ratio  $\mathcal{T}/|\mathcal{W} - \mathcal{M}|$  can be much smaller than 0.14 (mainly through the perturbation mode of the  $y_2$  branch), analogous to an unmagnetized composite SID system (Lou & Shen 2003). Shu et al. (2000) suggested a correspondence between  $\mathcal{T}/|\mathcal{W}|$  ratio and the onset of secular bar-like instabilities in a single fluid SID. It seems natural to extend this suggestion to a single MSID (Lou 2002) and to an unmagnetized composite system of two SIDs (Lou & Shen 2003). By this analogy, we now propose a further extension of this correspondence of

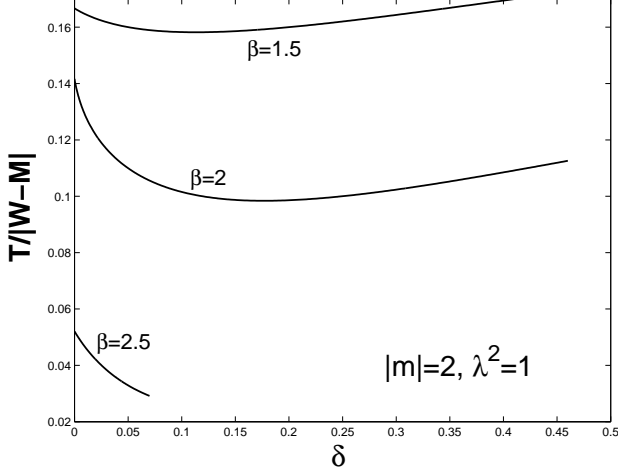


**Figure 8.** Curves of ratio  $\mathcal{T}/|\mathcal{W}-\mathcal{M}|$  versus  $\delta$  for different values of  $\beta = 1.5, 2, 2.5$  for the aligned  $|m| = 2$  case with  $\lambda^2 = 1$ .

ratio  $\mathcal{T}/|\mathcal{W}-\mathcal{M}|$  and the onset of secular bar-like instabilities in a composite system composed of one SID and one MSID. It then appears, as in the case of Lou & Shen (2003), the threshold of  $\mathcal{T}/|\mathcal{W}-\mathcal{M}|$  ratio can be considerably lowered in a composite SID or MSID system. Qualitatively, this illustrates that the mutual gravitational coupling tends to make a disc system more unstable (Jog & Solomon 1984a,b; Bertin & Romeo 1988; Romeo 1992; Elmegreen 1995; Jog 1996; Lou & Fan 1998b; Lou & Shen 2003; Shen & Lou 2003).

We now explore trends of variations for the ratio  $\mathcal{T}/|\mathcal{W}-\mathcal{M}|$  of the  $y_2$  branch. Setting  $|m| = 2$ , we present curves of  $\mathcal{T}/|\mathcal{W}-\mathcal{M}|$  versus  $\delta$  when parameters  $\beta$  and  $\lambda^2$  are specified (see Fig. 8). As there are three  $D_s^2$  solution branches involving three parameters  $\delta$ ,  $\beta$  and  $\lambda^2$ , values of ratio  $\mathcal{T}/|\mathcal{W}-\mathcal{M}|$  can be diversified. Consequently, instability properties of a composite (M)SIDs system are more complex than in a single SID. Moreover, possible perturbation modes of the  $D_s^2$  solution of  $y_2$  branch can vary with different values of azimuthal wavenumber  $|m|$  as shown in Figs. 9 and 10.

For parameters  $\delta = 0.2$ ,  $\beta = 1.5$  and  $\lambda^2 = 0.09$ ,  $D_s^2$  attains its minimum value around  $|m| = 9$ , while for parameters  $\delta = 0.2$ ,  $\beta = 1.2$  and  $\lambda^2 = 3.61$ , the minimum value of  $D_s^2$  occurs at  $|m| = 2$ . In association with the smallest value of  $D_s^2$ , the most vulnerable stationary perturbation configuration varies with chosen parameters. In other words, a slightly different choice of parameters may lead to entirely different MHD perturbation configurations. Again, this example shows the diversity and complexity in a composite MSID system and indicates that bar-like instabilities (i.e.  $m = 2$ ) may not necessarily be the dominant instability in a composite MSID system.

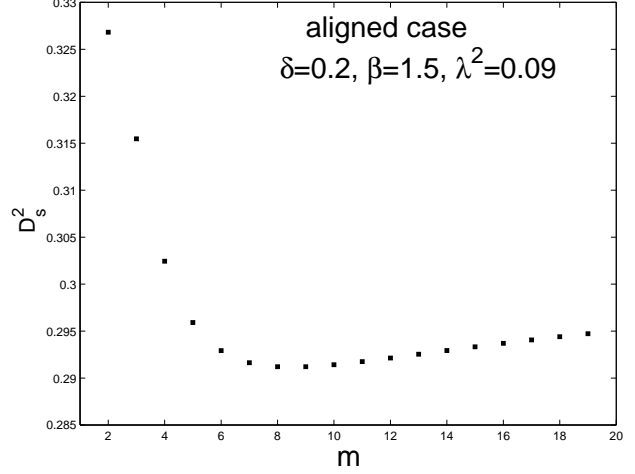


**Figure 9.** The  $D_s^2$  solution of the  $y_2$  branch versus  $|m|$  with parameters  $\delta = 0.2$ ,  $\beta = 1.5$  and  $\lambda^2 = 0.09$ . The smallest  $D_s^2$  occurs at  $|m| = 9$ .

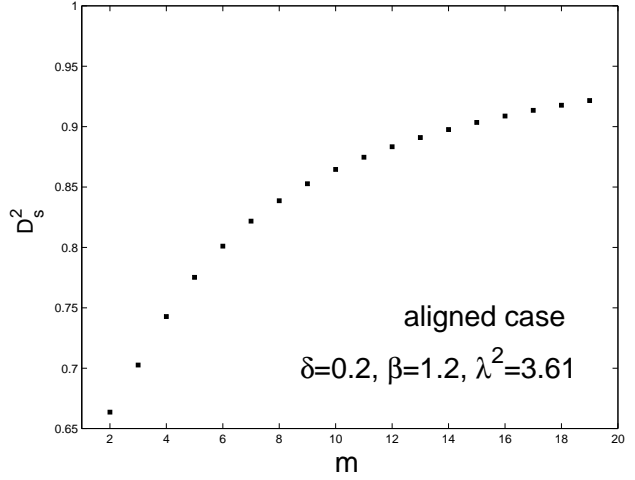


**Figure 10.** The  $D_s^2$  solution of the  $y_2$  branch versus  $|m|$  with parameters  $\delta = 0.2$ ,  $\beta = 1.2$  and  $\lambda^2 = 3.61$ . The smallest  $D_s^2$  occurs at  $|m| = 2$  in this case.

#### 4 UNALIGNED MHD PERTURBATIONS OF LOGARITHMIC SPIRALS

In this section, we analyze unaligned perturbation configurations of logarithmic spiral structures in a composite MSID system. We first derive the stationary dispersion relation for both full and partial composite MSID system. We then focus on the full case ( $F = 1$ ) and address the problem of axisymmetric marginal instabilities with  $|m| = 0$ .

##### 4.1 Stationary Dispersion Relation for Logarithmic Spirals

To construct stationary MHD perturbation configurations of unaligned logarithmic spirals in a composite MSID system, we pick the following potential-density pair (Syer & Tremaine 1996; Lynden-Bell & Lemos 1993; Shu et al. 2000;

Lou 2002; Lou & Fan 2002; Lou & Shen 2003), namely

$$\mu_s = \sigma_s r^{-3/2+i\alpha}, \quad (90)$$

$$\mu_g = \sigma_g r^{-3/2+i\alpha}, \quad (91)$$

where  $\sigma_s$  and  $\sigma_g$  are two constant coefficients and  $\alpha$  is the radial scaling parameter related effectively to the radial wavenumber, together with

$$V = v_s r^{-1/2+i\alpha} + v_g r^{-1/2+i\alpha}, \quad (92)$$

where the two constant coefficients  $v_s$  and  $v_g$  are related to  $\sigma_s$  and  $\sigma_g$  respectively by

$$v_s = -2\pi G \mathcal{N}_m(\alpha) \sigma_s, \quad (93)$$

$$v_g = -2\pi G \mathcal{N}_m(\alpha) \sigma_g, \quad (94)$$

with  $\mathcal{N}_m(\alpha) \equiv K(\alpha, m)$  being the Kalnajs function (Kalnajs 1971). Consistently, we may write

$$U_g = u_g r^{-1/2+i\alpha} \quad (95)$$

and

$$U_s = u_s r^{-1/2+i\alpha}, \quad (96)$$

where  $u_g$  and  $u_s$  are two constant coefficients. Using expressions (91), (92) and (95), equations (46), (47), (49) and (50) lead to

$$\begin{aligned} \frac{m\Omega_g\sigma_g}{\Sigma_0^g} + iu_g \left( i\alpha + \frac{C_A^2}{2\Omega_g^2 r^2} - \frac{3}{2} \right) \\ - \frac{m}{\Omega_g r} \left( \frac{a_g^2 \sigma_g}{r \Sigma_0^g} + v_s + v_g \right) = 0, \end{aligned} \quad (97)$$

$$\begin{aligned} \left\{ m^2 \Omega_g^2 r^2 - \kappa_g^2 r^2 - C_A^2 \left[ m^2 - 1 - \left( \frac{C_A^2}{2\Omega_g^2 r^2} - \frac{3}{2} \right) \right. \right. \\ \left. \left. \times \left( \frac{C_A^2}{2\Omega_g^2 r^2} - 2 \right) \right] \right\} iu_g = C_A^2 \left( i\alpha + 2 - \frac{C_A^2}{2\Omega_g^2 r^2} \right) \\ \times \left[ \frac{m\Omega_g\sigma_g}{\Sigma_0^g} - \frac{m}{\Omega_g r} \left( \frac{a_g^2 \sigma_g}{r \Sigma_0^g} + v_s + v_g \right) \right] \\ + m\Omega_g r \left( i\alpha + \frac{3}{2} \right) \left( \frac{a_g^2 \sigma_g}{r \Sigma_0^g} + v_s + v_g \right) - \frac{m\Omega_g C_A^2 \sigma_g}{2\Sigma_0^g}, \end{aligned} \quad (98)$$

$$iR = \frac{r^{1/2} B_\theta}{\Omega_g r} iu_g r^{-1+i\alpha} = \frac{B_\theta i U_g}{\Omega_g r}, \quad (99)$$

$$Z = -\frac{i\alpha r^{1/2} B_\theta}{m\Omega_g r} iu_g r^{-1+i\alpha} = -\frac{i\alpha B_\theta}{m\Omega_g r} iU_g. \quad (100)$$

A combination of equations (97) and (98) together with relations (93) and (94) give

$$\begin{aligned} \left[ \left( \frac{\mathcal{K}m}{\Omega_g r} - \mathcal{A} \right) \left( \frac{a_g^2}{r \Sigma_0^g} - 2\pi G \mathcal{N}_m(\alpha) \right) \right. \\ \left. - \left( \mathcal{C} + \frac{\mathcal{K}m\Omega_g}{\Sigma_0^g} \right) \right] \sigma_g = \left( \frac{\mathcal{K}m}{\Omega_g r} - \mathcal{A} \right) 2\pi G \mathcal{N}_m(\alpha) \sigma_s, \end{aligned} \quad (101)$$

where the three coefficients  $\mathcal{K}$ ,  $\mathcal{A}$  and  $\mathcal{C}$  are defined by

$$\mathcal{K} \equiv \left( m - \frac{2}{m} \right) \Omega_g r - \frac{(\alpha^2 + m^2 - 1)C_A^2}{m\Omega_g r}, \quad (102)$$

$$\mathcal{A} \equiv \frac{3}{2} \left( \frac{C_A^2}{2\Omega_g^2 r^2} - \frac{3}{2} \right) - \alpha^2, \quad (103)$$

$$\mathcal{C} \equiv -\frac{C_A^2}{2r\Sigma_0^g} \left( \frac{C_A^2}{2\Omega_g^2 r^2} - \frac{3}{2} \right). \quad (104)$$

For stationary coplanar perturbations in the stellar disk in parallel, we set  $\omega = 0$  in equations (37)–(39) and use equations (90)–(94) and (96) to obtain

$$\begin{aligned} \left[ \left( m^2 + \alpha^2 + \frac{1}{4} \right) \left( \frac{a_s^2}{r \Sigma_0^s} - 2\pi G \mathcal{N}_m(\alpha) \right) \right. \\ \left. - \frac{1}{r \Sigma_0^s} (m^2 - 2) \Omega_s^2 r^2 \right] \sigma_s \\ = \left( m^2 + \alpha^2 + \frac{1}{4} \right) 2\pi G \mathcal{N}_m(\alpha) \sigma_g. \end{aligned} \quad (105)$$

Equation (105) can also be obtained by setting  $C_A = 0$  in equation (101) and exchange subscripts  $s$  and  $g$ .

By equations (105) and (101), we derive

$$\begin{aligned} \frac{r}{\Omega_g^2 m^2} \left[ \frac{(m^2 - 2)}{r} \Omega_s^2 r^2 - \left( m^2 + \alpha^2 + \frac{1}{4} \right) \right. \\ \left. \times \left( \frac{a_s^2}{r} - 2\pi G \mathcal{N}_m(\alpha) \Sigma_0^s \right) \right] \times \left\{ m^4 \Omega_g^4 - m^2 \Omega_g^2 \left[ 2\Omega_g^2 \right. \right. \\ \left. \left. + \left( \frac{C_A^2 + a_g^2}{r^2} - \frac{2\pi G \mathcal{N}_m(\alpha) \Sigma_0^g}{r} \right) \left( m^2 + \alpha^2 + \frac{1}{4} \right) - \frac{2C_A^2}{r^2} \right] \right. \\ \left. + \frac{m^2 C_A^2}{r^2} \left[ \left( \frac{a_g^2}{r^2} - \frac{2\pi G \mathcal{N}_m(\alpha) \Sigma_0^g}{r} \right) \left( m^2 + \alpha^2 - \frac{1}{4} \right) \right. \right. \\ \left. \left. - \frac{C_A^2}{4r^2} \right] \right\} = 4\pi^2 G^2 \mathcal{N}_m^2(\alpha) \Sigma_0^s \Sigma_0^g \left( m^2 + \alpha^2 + \frac{1}{4} \right) \\ \times \left[ \left( m^2 + \alpha^2 + \frac{1}{4} \right) - \frac{C_A^2}{\Omega_g^2 r^2} \left( m^2 + \alpha^2 - \frac{1}{4} \right) \right]. \end{aligned} \quad (106)$$

In the absence of the gravitational coupling between the stellar SID and the gaseous MSID represented by the right-hand side term of equation (106), the left-hand side of dispersion relation (106) would be reduced to two separate dispersion relation factors. The first dispersion relation would be

$$\frac{(m^2 - 2)}{r} \Omega_s^2 r^2 - \left( m^2 + \alpha^2 + \frac{1}{4} \right) \left[ \frac{a_s^2}{r} - 2\pi G \mathcal{N}_m(\alpha) \Sigma_0^s \right] = 0 \quad (107)$$

for stationary logarithmic spirals in a single stellar SID without magnetic field. Substituting expressions (11) and (19) of  $\Omega_s$  and  $\Sigma_0^s$  with  $F = 1$  into equation (107), we have

$$\left( m^2 + \alpha^2 + \frac{1}{4} \right) \frac{[1 - (1 + D_s^2) \mathcal{N}_m(\alpha)]}{D_s^2 (m^2 - 2)} = 1, \quad (108)$$

which is simply equation (37) of Shu et al. (2000). The second dispersion relation would be

$$\begin{aligned} m^4 \Omega_g^4 - \left[ 2\Omega_g^2 + \left( \frac{C_A^2 + a^2}{r^2} - \frac{2\pi G \mathcal{N}_m(\alpha) \Sigma_0^g}{r} \right) \right. \\ \left. \times \left( m^2 + \alpha^2 + \frac{1}{4} \right) - \frac{2C_A^2}{r^2} \right] m^2 \Omega_g^2 + \frac{m^2 C_A^2}{r^2} \\ \times \left[ \left( \frac{a^2}{r^2} - \frac{2\pi G \mathcal{N}_m(\alpha) \Sigma_0^g}{r} \right) \left( m^2 + \alpha^2 - \frac{1}{4} \right) - \frac{C_A^2}{4r^2} \right] = 0 \end{aligned} \quad (109)$$

for stationary logarithmic spirals in a single gaseous MSID with coplanar magnetic field. Equation (109) is simply equation (3.4.15) of Lou (2002).

Without magnetic field with  $C_A = 0$ , equation (106) is equivalent to the dispersion relation (86) for stationary logarithmic spiral configurations in a composite SID system of Lou & Shen (2003) as it should be.

For numerical computations, there are two useful formulae of  $\mathcal{N}_m(\alpha)$ , namely, the recursion relation

$$\mathcal{N}_{m+1}(\alpha)\mathcal{N}_m(\alpha) = [(m+1/2)^2 + \alpha^2]^{-1} \quad (110)$$

and the asymptotic expansion

$$\mathcal{N}_m(\alpha) \approx (m^2 + \alpha^2 + 1/4)^{-1/2} \quad (111)$$

when  $m^2 + \alpha^2 \gg 1$  (Kalnajs 1971; Shu et al. 2000).

For the purpose of examining phase relationship between the azimuthal magnetic field perturbation  $b_\theta$  and the surface mass density perturbation  $\Sigma_g^1$  of the gaseous MSID in the full case of  $F = 1$ , we derive the following relations. From equations (97) and (105) with  $F = 1$ , we readily obtain

$$iu_g = \frac{2\pi G m \sigma_g}{[i\alpha + C_A^2/(2\Omega_g^2 r^2) - 3/2](\Omega_g r)} \times \left[ \frac{(1+\delta)(1-D_g^2)}{\delta(1+D_g^2-\lambda^2/2)} - \frac{\mathcal{A}\mathcal{N}_m(\alpha)}{(\mathcal{A}-\mathcal{B})} \right], \quad (112)$$

where the two coefficients  $\mathcal{A}$  and  $\mathcal{B}$  are defined by

$$\mathcal{A} \equiv (m^2 + \alpha^2 + 1/4) - (m^2 - 2)D_s^2 \quad (113)$$

and

$$\mathcal{B} \equiv \frac{\mathcal{N}_m(\alpha)}{(1+\delta)}(m^2 + \alpha^2 + 1/4)(1+D_s^2). \quad (114)$$

It follows from expressions (100) and (112) that

$$\frac{Z}{\mu_g} \propto \left[ \alpha^2 + i\alpha \left( \frac{\lambda^2}{2D_g^2} - \frac{3}{2} \right) \right] \times \left[ \frac{(1+\delta)(1-D_g^2)}{\delta(1+D_g^2-\lambda^2/2)} - \frac{\mathcal{A}\mathcal{N}_m(\alpha)}{(\mathcal{A}-\mathcal{B})} \right], \quad (115)$$

that will be discussed later in our analysis.

#### 4.2 Marginal Stability for Axisymmetric Disturbances

While the  $|m| = 0$  case is somewhat trivial as a rescaling in the aligned case, it is of considerable interest in the special ‘spiral’ case with radial oscillations. In this subsection, we analyze this situation for a full composite MSID system with  $F = 1$ . A substitution of expressions (11), (14), (19) and (20) into equation (106) with  $\lambda^2 \equiv C_A^2/a_g^2$  leads to

$$\begin{aligned} & \left\{ -2D_s^2 - \left( \alpha^2 + \frac{1}{4} \right) \left[ 1 - \frac{\mathcal{N}_0(\alpha)(1+D_s^2)}{1+\delta} \right] \right\} \\ & \times \left\{ -D_g^2 \left[ 2D_g^2 + \left( \lambda^2 + 1 - \frac{\mathcal{N}_0(\alpha)(1+D_g^2-\lambda^2/2)\delta}{1+\delta} \right) \right] \right. \\ & \times \left( \alpha^2 + \frac{1}{4} \right) - 2\lambda^2 \left[ \left( 1 - \frac{\mathcal{N}_0(\alpha)(1+D_g^2-\lambda^2/2)\delta}{1+\delta} \right) \right. \\ & \times \left( \alpha^2 - \frac{1}{4} \right) - \frac{\lambda^2}{4} \left. \right] \left. \right\} - \frac{\mathcal{N}_0(\alpha)^2 D_g^2 (1+D_s^2)(1+D_g^2-\lambda^2/2)\delta}{(1+\delta)^2} \\ & \times \left( \alpha^2 + \frac{1}{4} \right) \left[ \alpha^2 + \frac{1}{4} - \lambda^2 \left( \alpha^2 - \frac{1}{4} \right) / D_g^2 \right] = 0. \end{aligned} \quad (116)$$

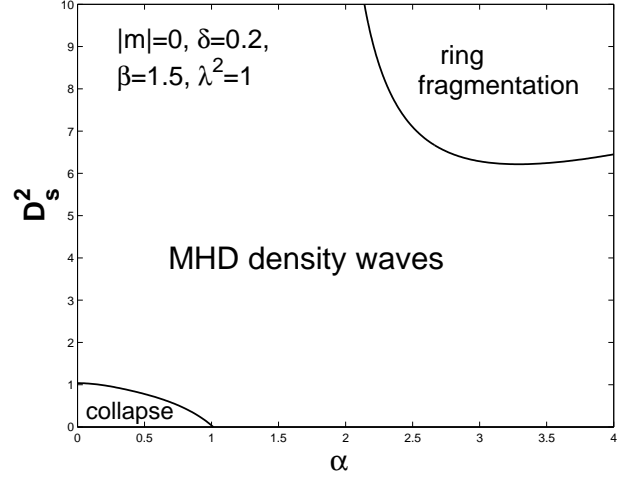


**Figure 11.** The marginal stability curve of  $D_s^2$  versus  $\alpha$  with  $m = 0$ ,  $\delta = 0.2$ ,  $\beta = 1.5$  and  $\lambda^2 = 1$ .

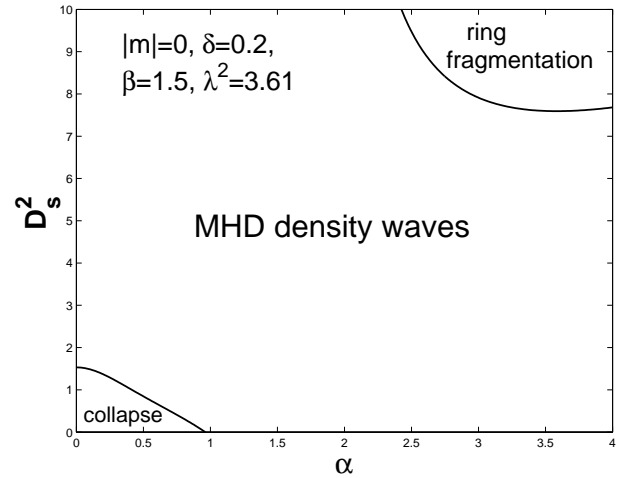


**Figure 12.** The marginal stability curve of  $D_s^2$  versus  $\alpha$  with  $m = 0$ ,  $\delta = 0.2$ ,  $\beta = 1.5$  and  $\lambda^2 = 3.61$ .

By recursion formula (110) and asymptotic expression (111) for the Kalnajs functions, we have an approximate expression of  $\mathcal{N}_0(\alpha)$ , namely

$$\begin{aligned} \mathcal{N}_0(\alpha) &= (\alpha^2 + 9/4)/(\alpha^2 + 1/4)\mathcal{N}_2(\alpha) \\ &= (\alpha^2 + 9/4)/[(\alpha^2 + 1/4)(\alpha^2 + 17/4)^{1/2}]. \end{aligned} \quad (117)$$

A substitution of approximate expression (117) for  $\mathcal{N}_0(\alpha)$  and expression (23) for  $D_g^2$  into dispersion relation (116) yields a cubic algebraic equation in terms of  $D_s^2$ ; and similarly, a substitution of approximate expression (117) for  $\mathcal{N}_0(\alpha)$  and expression (24) for  $D_s^2$  yields another cubic algebraic equation in terms of  $D_g^2$ . As noted earlier, we consider the cubic equation of  $D_s^2$  because of the fact that  $D_s^2 < D_g^2$  when  $\beta \geq 1$ . For different values of parameters  $\delta$ ,  $\beta$  and  $\lambda^2$ , we show curves of  $D_s^2$  versus  $\alpha$  in Figs. 11–15.

For the positive portions of solution  $D_s^2$  with typical parameters, it turns out that the basic features of a  $D_s^2$  versus  $\alpha$  profile are qualitatively similar to those of a single SID [see fig. 2 of Shu et al. (2000)] and to those of a composite

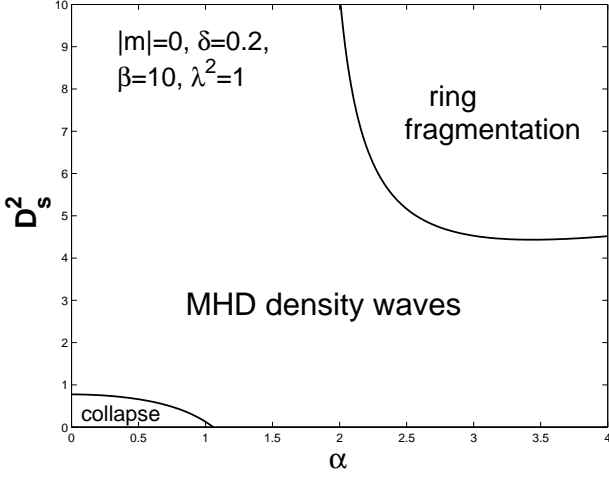


**Figure 13.** The marginal stability curve of  $D_s^2$  versus  $\alpha$  with  $m = 0$ ,  $\delta = 0.2$ ,  $\beta = 10$  and  $\lambda^2 = 1$ .

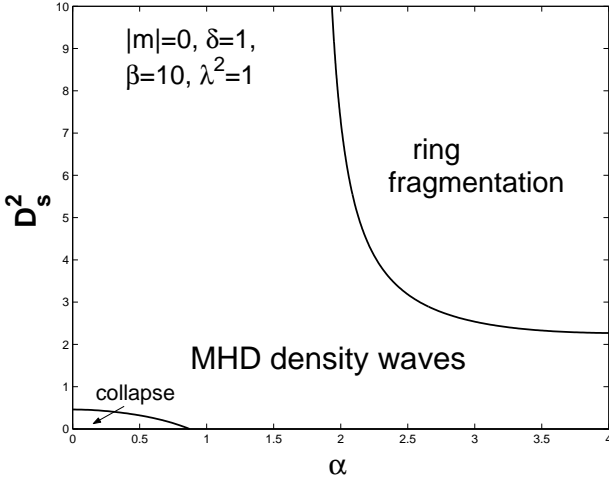


**Figure 14.** The marginal stability curve of  $D_s^2$  versus  $\alpha$  with  $m = 0$ ,  $\delta = 1$ ,  $\beta = 10$  and  $\lambda^2 = 1$ .

SID system (see figs. 5 – 10 of Lou & Shen 2003), except that now trends of variation for  $D_s^2$  with three parameters become more complicated. For example, the lower ring fragmentation curve first discussed in a single MSID (Lou 2002) becomes negative or indiscernible in most cases (see Appendix B). For cases of  $\beta$  around 1, however, the lower ring fragmentation curve of  $D_s^2$  may become positive as shown in Fig. 15.

As parameters  $\delta$ ,  $\beta$  and  $\lambda^2$  vary, we note several trends of variation in the profiles of  $D_s^2$ . For example, when  $\lambda^2$  increases for fixed  $\delta$  and  $\beta$ , the ring fragmentation curves of  $D_s^2$  seem to be raised, and the collapse regime tends to be enlarged by comparing Figs. 11 and 12. In other words, the presence of coplanar magnetic field tends to increase the chance of collapse but reduce the danger of ring fragmentation. This feature is qualitatively similar to the case of a single coplanar magnetized SID studied by Lou (2002) (see fig. 1 of Lou 2002). As  $\beta$  increases for fixed  $\delta$  and  $\lambda^2$ ,

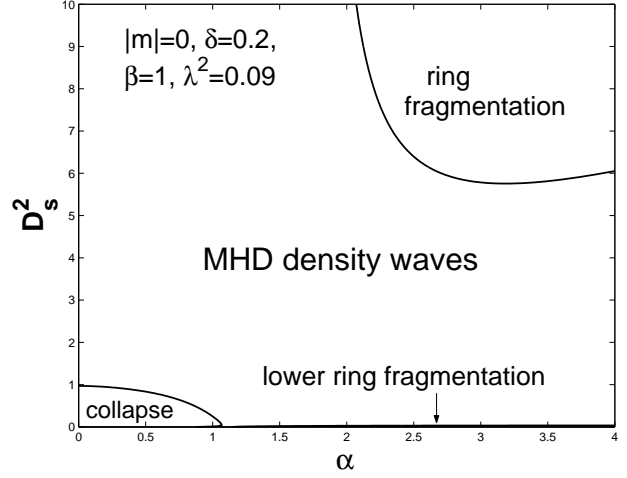


**Figure 15.** The marginal stability curve of  $D_s^2$  versus  $\alpha$  with  $m = 0$ ,  $\delta = 0.2$ ,  $\beta = 1$  and  $\lambda^2 = 0.09$ . For  $\beta \rightarrow 1$ , the lower ring fragmentation branch would gradually rise above the horizontal  $\alpha$  axis.

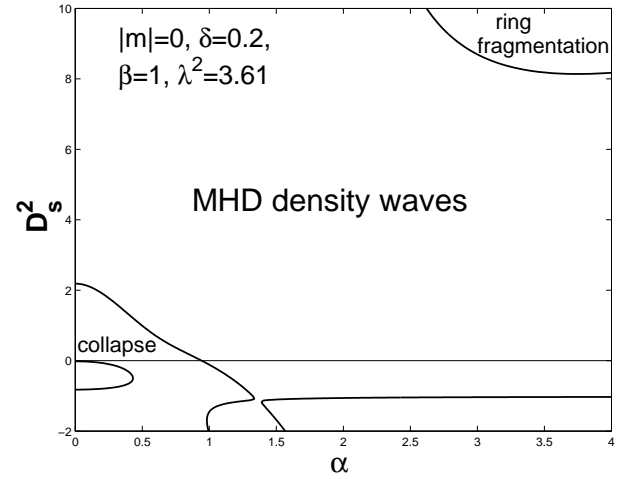


**Figure 16.** The marginal stability curve of  $D_s^2$  versus  $\alpha$  with  $m = 0$ ,  $\delta = 0.2$ ,  $\beta = 1$  and  $\lambda^2 = 3.61$ . Compared with Fig. 15, the increase of  $\lambda$  moves the lower ring fragmentation downward.

the curves of  $D_s^2$  tend to be lowered by comparing Figs. 11 and 13. When  $\delta$  increases for fixed  $\beta$  and  $\lambda^2$ , the ring fragmentation curves of  $D_s^2$  decrease, and the collapse regime shrinks by comparing Figs. 13 and 14. Note that as  $\delta$  increases ( $\delta \equiv \Sigma_0^g / \Sigma_0^s$ ), the influence of gas disc on the stellar disc becomes more important. Therefore, the gravitational coupling with another disc tends to suppress the collapse but enhance the danger of ring fragmentation.

One behaviour for the variation of the lower ring fragmentation curve appears somewhat surprising. It seems to be a characteristic feature involving magnetic field (Lou 2002). As already noted earlier, when  $\beta$  approaches 1, this curve could rise above the  $\alpha$  axis to become a possible perturbation mode (Fig. 15). However, comparing Fig. 15 with Fig. 16, we find that in typical parameter regimes, the increase of  $\lambda$  would force the lower ring fragmentation curve

to go downward. This is completely different from that of a single MSID (see fig. 1 of Lou 2002).

Through numerical explorations, we realize that the location  $\alpha$  of the vertical asymptote for the ring fragmentation branch seems to be independent of  $\delta$ ,  $\beta$  and  $\lambda^2$ . By letting the coefficient of the cubic term in the cubic algebraic equation of  $y \equiv D_s^2$  to vanish, the condition that this critical value  $\alpha_c$  must satisfy is once again

$$\mathcal{N}_0(\alpha)(\alpha^2 + 1/4) = 2, \quad (118)$$

which is exactly the same as that of Shu et al. (2000), Lou (2002) and Lou & Shen (2003) for three related but different SID systems. From equation (117) and asymptotic expansion (111), this critical value  $\alpha_c$  is estimated to be 1.759.

Physical interpretations for the marginal instability curves are clear. As  $\alpha$  parameter is a measure for the radial wavenumber, a smaller  $\alpha$  corresponds to a larger radial scale of perturbations. Thus, the collapse regime indicates a rotationally modified Jeans instability to which a composite MSID system is vulnerable when a radial perturbation scale is sufficiently large (i.e. a sufficiently small  $\alpha$ ). However, when  $D_s^2$  becomes larger, the conservation of angular momentum works against the inward gravitational force and the Jeans instability is suppressed.

Nevertheless, a composite MSID system is also vulnerable to Toomre-type instability (Safronov 1960; Toomre 1964) associated with the ring fragmentation branch (Shu et al. 2000). In various galactic contexts, there have been numerous studies to identify an effective  $Q$  parameter for a composite disc system (Jog & Solomon 1984a,b; Bertin & Romeo 1988; Kennicutt 1989; Romeo 1992; Elmegreen 1995; Jog 1996; Lou & Fan 1998b). In the case of a single SID, Shu et al. (2000) noted that the minimum of the ring fragmentation curve is closely related to the Toomre  $Q$  parameter (Toomre 1964). In the case of a coplanar magnetized SID, Lou (2002) and Lou & Fan (2002) further found that the minimum of the upper ring fragmentation curve is tightly associated with the generalized MHD  $Q_M$  parameter (Lou & Fan 1998a). For a composite system of two SIDs, Shen & Lou (2003) recently suggested a straightforward  $D$ -criterion to effectively determine the axisymmetric stability against ring fragmentation (see Elmegreen 1995 and Jog 1996 for other proposed criteria). We therefore expect that in the present problem, the minimum of the upper ring fragmentation curve should be related a magnetic field modified  $D$ -criterion to effectively determine the axisymmetric stability against ring fragmentation in a composite system of one fluid SID and one MSID.

### 4.3 Stationary Logarithmic Spiral Configurations

#### 4.3.1 Behaviours of $D_s^2$ solutions

Parallel to the study of aligned  $|m| \geq 2$  cases, we substitute expressions (11), (14), (19), (20) and (23) into equation (106) with  $\lambda^2 \equiv C_A^2/a_g^2$  and obtain a cubic algebraic equation of  $y \equiv D_s^2$  for unaligned spiral cases. One can formally derive three analytic  $D_s^2$  solutions (see Appendix D) that would

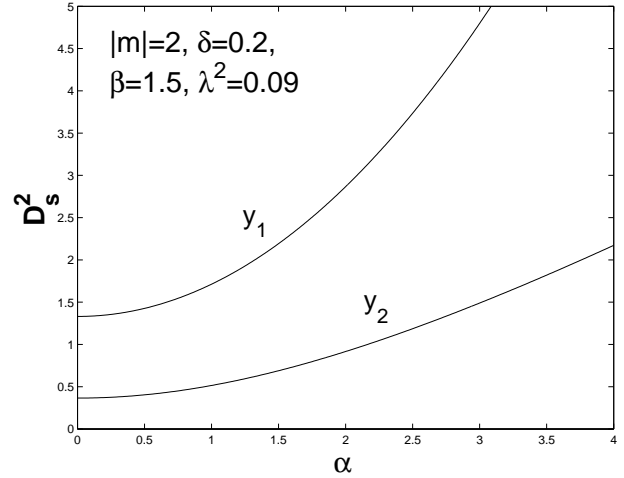


**Figure 17.** Curves of  $D_s^2$  versus  $\alpha$  for a stationary unaligned logarithmic spiral with  $|m| = 2$ ,  $\delta = 0.2$ ,  $\beta = 1.5$  and  $\lambda^2 = 0.09$ .

be valuable in numerical MHD simulation studies of large-scale SID dynamics within the overall MHD density-wave scenario.

To explore parameter regimes, we obtain  $D_s^2$  solution curves numerically for cases of  $|m| = 1, 2, 3, \dots$  and so forth. As expected, there are three solution curves of  $D_s^2$  versus  $\alpha$  given parameters  $|m|$ ,  $\delta$ ,  $\lambda^2$  and  $\beta$ . In certain parameter regimes, portions of the lower two  $D_s^2$  solution curves may become negative and hence unphysical. We defer our discussion of  $|m| = 1$  case later. In Figs. 17–19, we show a set of numerical examples with  $|m| = 2$ . Through extensive numerical examples of stationary logarithmic spiral cases from  $|m| = 2$  to  $|m| = 5$ , it is clear that behaviours of  $D_s^2$  solutions and properties of phase relationships among perturbation variables for  $|m| > 2$  cases are very similar to those of  $|m| = 2$  logarithmic spiral. We therefore carefully examine the  $|m| = 2$  spiral case for a relatively simple yet meaningful analysis. In addition, we plot curves of  $D_s^2$  versus  $\beta$  by specifying  $\alpha$ ,  $\delta$  and  $\lambda^2$  in Fig. 20.

As in the aligned case, we shall use  $y_1$ ,  $y_2$  and  $y_3$  to denote the upper, middle and lower solution branches, respectively. It is apparent that the three  $D_s^2$  solution branches do not intersect with each other. Similar to the case of axisymmetric disturbances, the lowest  $y_3$  solution branch does not appear above zero in many cases, but for cases with relatively small  $\beta$  value (e.g.  $\beta = 1$ ),  $y_3$  solution branch can become a possible stationary perturbation mode (see Figs. 19 and 20). We note that  $D_s^2$  always increases with increasing  $\alpha$  for the upper two branches  $y_1$  and  $y_2$  (see Figs. 17–19) but decreases with increasing  $\beta$  (see Fig. 20). The uppermost  $y_1$  branch may cross the horizontal  $\alpha$  axis to become negative in some cases (see Fig. 18), similar to the situation without involving coplanar magnetic field (Lou & Shen 2003).

In Fig. 20, there exist a  $\beta_{c1}$  for the middle  $y_2$  branch and a  $\beta_{c2}$  for the lowest  $y_3$  branch for given  $\alpha$ ,  $\delta$  and  $\lambda^2$  such that  $y_2$  and  $y_3$  become zero and negative with increasing value

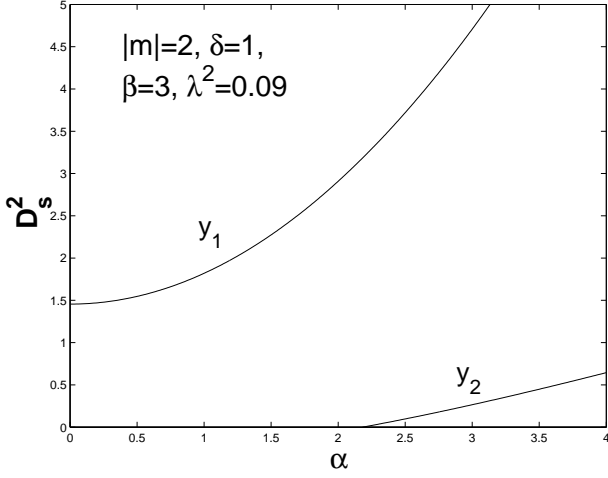


**Figure 18.** Curves of  $D_s^2$  versus  $\alpha$  for a stationary unaligned logarithmic spiral with  $|m| = 2$ ,  $\delta = 1$ ,  $\beta = 3$  and  $\lambda^2 = 0.09$ .

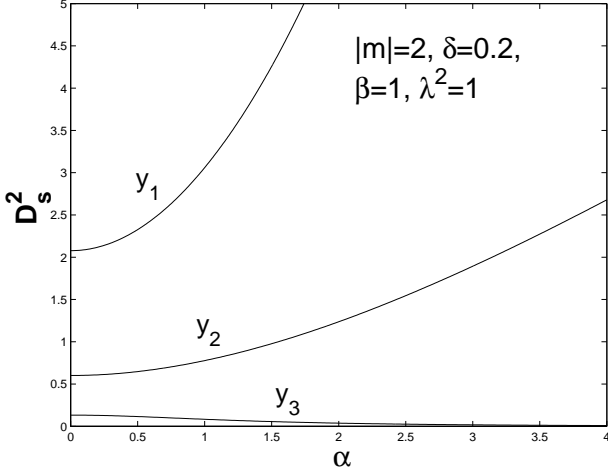


**Figure 19.** Curves of  $D_s^2$  versus  $\alpha$  for a stationary unaligned logarithmic spiral with  $|m| = 2$ ,  $\delta = 0.2$ ,  $\beta = 1$  and  $\lambda^2 = 1$ .

of  $\beta$ , respectively. Parallel to the aligned case, we examine behaviours of the solutions and obtain the two critical values of  $\beta$  analytically. For the  $|m| = 2$  case, the analytic forms of  $\beta_{c1}$  and  $\beta_{c2}$  are given by

$$\beta_{c1} = \frac{1}{2\mathcal{A}}[-\mathcal{B} + (\mathcal{B}^2 - 4\mathcal{A}\mathcal{C})^{1/2}] \quad (119)$$

and

$$\beta_{c2} = \frac{1}{2\mathcal{A}}[-\mathcal{B} - (\mathcal{B}^2 - 4\mathcal{A}\mathcal{C})^{1/2}], \quad (120)$$

where definitions of the three coefficients  $\mathcal{A}$ ,  $\mathcal{B}$  and  $\mathcal{C}$  are given in Appendix A. When  $\beta < \beta_{c1}$ , the middle solution branch  $y_2 \equiv D_s^2$  is positive, while for  $\beta > \beta_{c1}$ , the middle solution branch  $y_2 \equiv D_s^2$  becomes negative and hence unphysical. For the case of  $\delta = 0.2$ ,  $\lambda^2 = 0.09$  and  $\alpha = 0$ , we obtain  $\beta_{c1} = 2.409$  from equation (119), consistent with Fig. 17; in Fig. 17, we have  $\beta = 1.5 < \beta_{c1}$  and the middle branch  $y_2$  is positive at  $\alpha = 0$ . For  $\lambda^2 = 1.00$ , expressions (119) and (120) give  $\beta_{c1} = 2.468$  and  $\beta_{c2} = 1.140$ , respectively, consistent with Fig. 20.

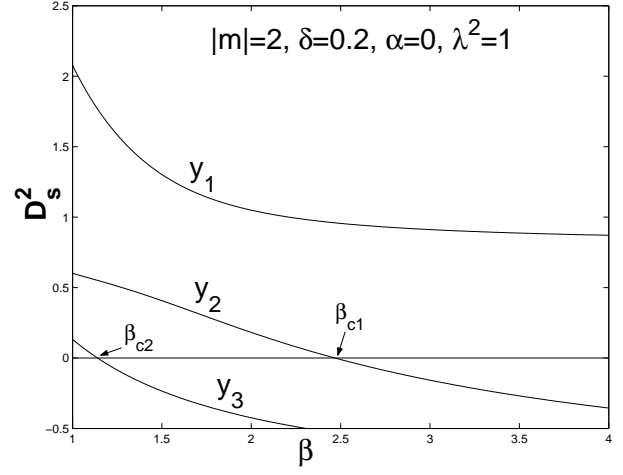


**Figure 20.** Curves of  $D_s^2$  versus  $\beta$  for a stationary unaligned logarithmic spiral with  $|m| = 2$ ,  $\delta = 0.2$ ,  $\alpha = 0$  and  $\lambda^2 = 1$ .

#### 4.3.2 Phase relationships among perturbation variables

For stationary logarithmic perturbation spirals, we now examine spatial phase relationships between perturbations of the surface mass densities of the two SIDs (i.e.  $\mu_g$  and  $\mu_s$ ), and between perturbations of the azimuthal magnetic field and the surface mass density of the gaseous MSID (i.e.  $b_\theta$  and  $\Sigma_1^g$ ). This information might provide necessary and useful clues for optical and synchrotron radio observational diagnostics of spiral galaxies.

From equation (105), one obtains

$$\begin{aligned} \frac{\mu_g}{\mu_s} &= (m^2 + \alpha^2 + 1/4)^{-1} \mathcal{N}_m(\alpha)^{-1} \\ &\times \left\{ (m^2 + \alpha^2 + 1/4) \left[ \frac{(1+\delta)}{(1+y)} - \mathcal{N}_m(\alpha) \right] \right. \\ &\quad \left. - \frac{(m^2 - 2)(1+\delta)y}{1+y} \right\} \end{aligned} \quad (121)$$

with  $y \equiv D_s^2$ . Substitution of expression (121) into the cubic equation of  $D_s^2$  gives a cubic equation of  $\mu_g/\mu_s$ , and we plot several curves of  $\mu_g/\mu_s$  versus  $\beta$  with parameters  $\alpha = 1$ ,  $\delta = 0.2$ ,  $\lambda^2 = 0.09$  and 3.61 in Figs. 21 and 22.

For the phase relationship between  $\mu_g$  and  $Z$ , we start from equation (115). For a sufficiently small  $\alpha$ , corresponding to a relatively open spiral structure, one may keep linear terms of  $\alpha$  and ignore the  $\alpha^2$  term. It follows that  $Z$  is either ahead of or lagging behind  $\mu_g$  with a phase difference of about  $\sim \pi/2$ . On the other hand, for a sufficiently large  $\alpha$  in the tight-winding or WKB regime, one may drop the imaginary part in equation (115) (see Lou 2002). When accuracy is not that crucial in a quantitative analysis, this expression may also be roughly used in cases of  $\alpha \simeq 1$ . We can rewrite expression (115) approximately as

$$\frac{\mu_g}{Z} \propto \left\{ \alpha^2 \left[ \frac{(1+\delta)(1-D_g^2)}{\delta(1+D_g^2 - \lambda^2/2)} - \frac{\mathcal{A}\mathcal{N}_m(\alpha)}{\mathcal{A} - \mathcal{B}} \right] \right\}^{-1}, \quad (122)$$

where  $\mathcal{A}$  and  $\mathcal{B}$  are defined by equations (113) and (114), respectively. When parameters  $\alpha$ ,  $\beta$ ,  $\delta$  and  $\lambda^2$  are specified in equation (122), solutions of  $y \equiv D_s^2$  correspond to val-



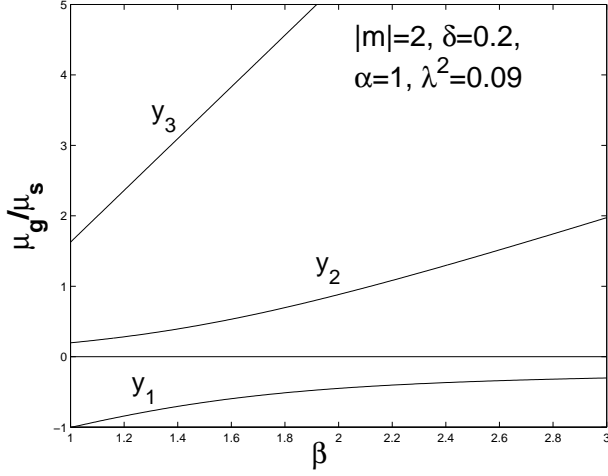


**Figure 21.** Curves of  $\mu_g/\mu_s$  versus  $\beta$  for a stationary logarithmic spiral with  $|m| = 2$ ,  $\delta = 0.2$ ,  $\alpha = 1$  and  $\lambda^2 = 0.09$ .

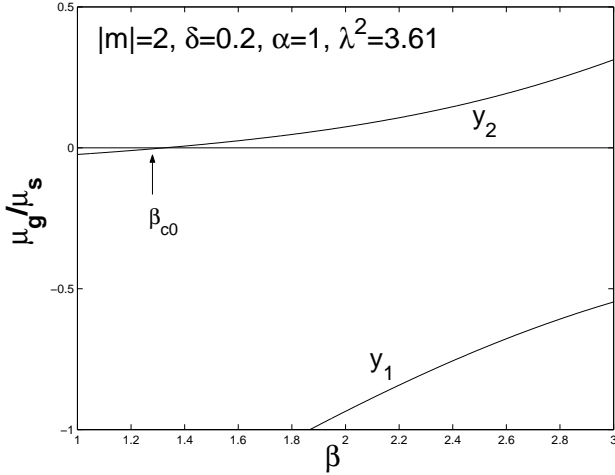


**Figure 22.** Curves of  $\mu_g/\mu_s$  versus  $\beta$  for a stationary logarithmic spiral  $|m| = 2$ ,  $\delta = 0.2$ ,  $\alpha = 1$  and  $\lambda^2 = 3.61$ . The uppermost branch corresponding to  $y_3 \equiv D_s^2$  is only discernible for  $\beta < 1$  and is not shown here. The branch corresponding to  $y_2 \equiv D_s^2$  may cross the horizontal  $\beta$  axis.

ues of  $\mu_g/Z$ . We then present curves of  $\mu_g/Z$  versus  $\beta$  with parameters  $\alpha = 1$ ,  $\delta = 0.2$ ,  $\lambda^2 = 0.09$  and  $3.61$  in Figs. 23 and 24. By equation (121), we note again that a smaller  $\mu_g/\mu_s$  corresponds to a larger  $y \equiv D_s^2$ , reminiscent of the same variation trend of correspondence in the aligned case described in Section 3. Such a relatively simple correspondence does not hold for  $\mu_g/Z$  that should be analyzed with extra care. Through extensive numerical explorations, we note that the highest branch of  $\mu_g/Z$  always relates to the lowest  $y_3$  branch, while the  $y_1$  branch of  $\mu_g/Z$  (being always negative) does not remain always less than the  $y_2$  branch of  $\mu_g/Z$  as shown in Figs. 23 and 24. These phase relationships among branches of  $\mu_g/\mu_s$  and  $\mu_g/Z$  and the corresponding branches of  $y \equiv D_s^2$  are shown explicitly in Figs. 21–24.

The unaligned spiral cases here are fairly similar to the aligned cases of Section 3, except that the imaginary part of

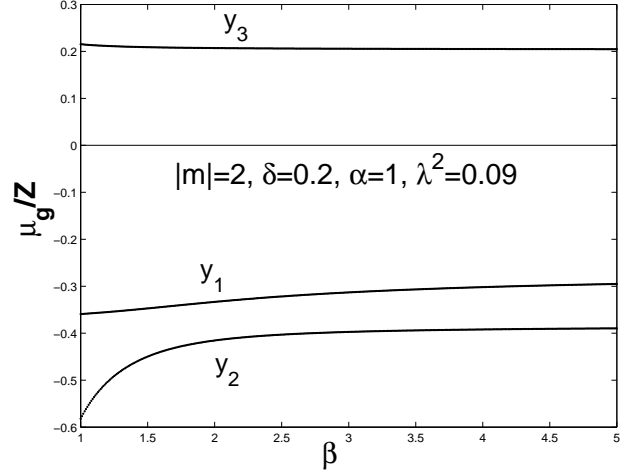


**Figure 23.** Curves of real parts of  $\mu_g/Z$  versus  $\beta$  for a stationary logarithmic spiral of  $|m| = 2$ ,  $\delta = 0.2$ ,  $\alpha = 1$  and  $\lambda^2 = 0.09$ . Imaginary parts of  $\mu_g/Z$  are not shown here. While one branch of real part of  $\mu_g/Z$  corresponding to  $y_1$  remains always negative, this branch does not remain always lower than the real part of  $\mu_g/Z$  branch corresponding to  $y_2$ .

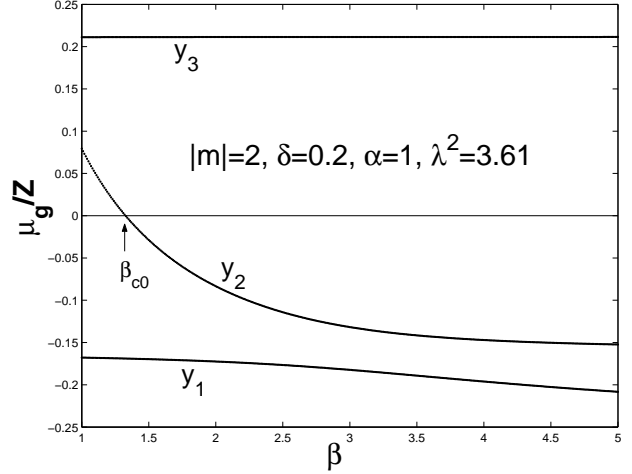


**Figure 24.** Curves of real parts of  $\mu_g/Z$  versus  $\beta$  for a stationary logarithmic spiral of  $|m| = 2$ ,  $\delta = 0.2$ ,  $\alpha = 1$  and  $\lambda^2 = 3.61$ . Imaginary parts of  $\mu_g/Z$  are not shown here. The uppermost branch for real part of  $\mu_g/Z$  is only discernible for  $\beta < 1$  and is not shown here. The branch of real part of  $\mu_g/Z$  corresponding to  $y_2 \equiv D_s^2$  may cross the horizontal  $\beta$  axis.

$\mu_g/Z$  does not vanish in general. For the stationary mode of  $y_1$  branch, the phase relationship between the surface mass density of the two SIDs (i.e.  $\mu_g/\mu_s$ ) and the phase relationship between the surface mass density of the MSID and the azimuthal magnetic field (i.e.  $\mu_g/Z$ ) are always out of phase (see Figs. 21–24).<sup>†</sup>

<sup>†</sup> To be more precise,  $\mu_g/Z$  being ‘out of phase’ means that the real part of  $\mu_g/Z$  is negative. As  $\alpha$  ranges from sufficiently small to relatively large values, the phase difference between  $\mu_g$  and  $Z$  ranges from  $\pi/2$  to  $\pi$ , either ahead or lagging behind. Likewise,  $\mu_g/Z$  being ‘in phase’ implies that the phase difference between

For the unaligned perturbation mode of  $y_2$  branch in most cases,  $\mu_g/\mu_s$  is in phase, while the real part of  $\mu_g/Z$  is always negative. Taking into account of the imaginary part of  $\mu_g/Z$ , the phase difference between  $\mu_g$  and  $Z$  is  $\pi/2 \sim \pi$  (see Figs. 21 and 23). This  $y_2$  branch has a zero point at  $\beta_{c0}$  (where  $\mu_g = 0$ ) that increases with increasing  $\lambda^2$ . When  $\lambda^2$  becomes sufficiently large (e.g.  $\lambda^2 = 3.61$ ) with  $\beta > 1$ , the value of  $\beta_{c0}$  can become larger than 1. It is then possible for  $\mu_g/\mu_s$  and  $\mu_g/Z$  to become zero at  $\beta = \beta_{c0}$  and reverse their respective signs for  $1 < \beta < \beta_{c0}$  as shown in Figs. 22 and 24. Taking into account of the imaginary part of  $\mu_g/Z$ , this implies that the phase difference of  $\mu_g$  and  $Z$  switch from between  $\pi/2 \sim \pi$  to between  $0 \sim \pi/2$  as  $\beta$  varies from  $\beta > \beta_{c0}$  to  $\beta < \beta_{c0}$ . Meanwhile during the same  $\beta$  transition, the phase difference between  $\mu_s$  and  $\mu_g$  switch from in phase to out of phase. The special situation of  $\mu_g = 0$  at  $\beta = \beta_{c0}$ , occurring for stationary perturbation mode of  $y_2$  branch, is very similar to that of the aligned case studied earlier. With  $\mu_g = J_g = 0$  but  $\mu_s \neq 0$ ,  $Z \neq 0$ ,  $\Phi_g \neq 0$  and  $U_g \neq 0$ , this may correspond to a unique solution.

For the stationary perturbation mode of  $y_3$  branch, both  $\mu_g/\mu_s$  and the real part of  $\mu_g/Z$  remain positive and therefore  $\mu_g$  and  $\mu_s$  are always in phase (see Figs. 21–24); taking into account of the imaginary part of  $\mu_g/Z$ , the phase difference between  $\mu_g$  and  $Z$  ranges from 0 to  $\pi/2$ .

The analytic expression of  $\beta_{c0}$  for  $|m| = 2$  and  $\alpha = 1$  is given by

$$\beta_{c0} = \frac{1}{609(1+\delta)} [\lambda^2(17\sqrt{21} + 68\delta + 68) + 168\delta + 42\sqrt{21} + 168], \quad (123)$$

that increases with increasing  $\lambda^2$ . For  $\delta = 0.2$  and  $\lambda^2 = 0.09$  in equation (123), one has  $\beta_{c0} = 0.5589$  that is not shown explicitly in Figs. 21 and 23 (see Fig. E1 in Appendix E). For  $\delta = 0.2$  and  $\lambda^2 = 3.61$ , one has  $\beta_{c0} = 1.3271$ , consistent with Figs. 22 and 24.

#### 4.3.3 Solution behaviours of unaligned $|m| = 1$ case

We now turn to the somewhat special case of  $|m| = 1$ . Mathematically, the qualitative difference between cases of  $|m| = 1$  and  $|m| \geq 2$  is perhaps due to the fact that  $\mathcal{N}_m(\alpha) < 1$  for  $|m| \geq 2$  but otherwise for  $|m| = 1$  (Lou & Shen 2003). We now examine behaviours of  $y \equiv D_s^2$  of the  $|m| = 1$  case shown in Figs. 25 and 26.

It turns out that solution curves of  $|m| = 1$  case indeed differ from those of  $|m| = 2$  case. For example, the middle and lower branches of  $y \equiv D_s^2$  remain always negative and hence unphysical (see Figs. 25 and 26). Portions of the upper branch of  $y_1 \equiv D_s^2$  may become zero or even negative for a sufficiently large  $\beta$  (Fig. 25). That is, when  $\beta$  exceeds a critical value  $\beta_{c3}$ ,  $y_1 \equiv D_s^2$  would become negative. The analytical form of this critical  $\beta_{c3}$  is given expression (124).

$\mu_g$  and  $Z$  ranges from 0 to  $\pi/2$  as  $\alpha$  varies from relatively large to sufficiently small values.

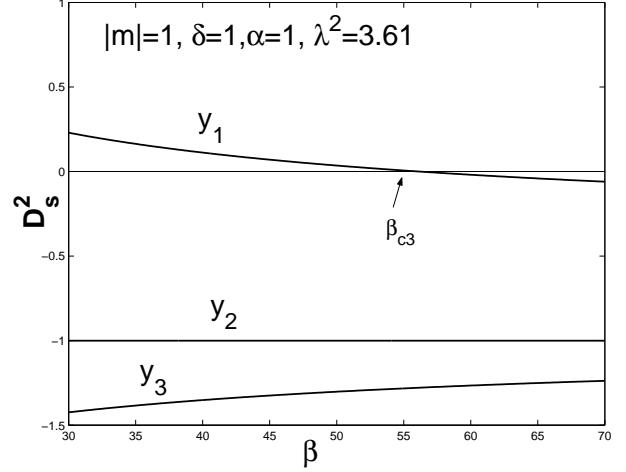


**Figure 25.** Curves of  $y \equiv D_s^2$  versus  $\beta$  for stationary unaligned perturbations of  $|m| = 1$  with  $\delta = 1$ ,  $\alpha = 1$  and  $\lambda^2 = 3.61$ . Solution branch of  $y_1 \equiv D_s^2$  may go across the horizontal  $\beta$  axis and has a root at about 56.

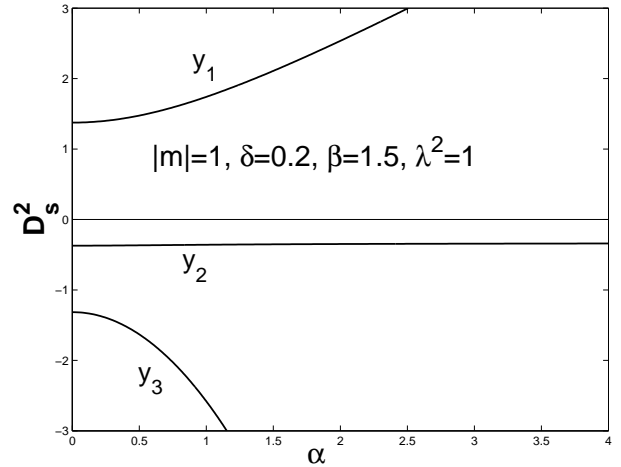


**Figure 26.** Curves of  $y \equiv D_s^2$  versus  $\alpha$  for stationary unaligned perturbations of  $|m| = 1$  with  $\delta = 0.2$ ,  $\beta = 1.5$  and  $\lambda^2 = 1$ .

These properties are similar to those in the case of a composite unmagnetized SID system studied by Lou & Shen (2003). The three solution branches of  $y \equiv D_s^2$  do not intersect with each other. The increase of  $\beta$  moves both  $y_1$  and  $y_2$  branches downward (see Fig. 25) and slightly lifts the lowest  $y_3$  branch.

One can derive an expression for the critical point of  $\beta$  where  $y_1 = 0$ . For  $\alpha = 1$ , the analytical form of this  $\beta_{c3}$  is

$$\beta_{c3} \equiv \frac{1}{(12\delta - 8)} [1 + 21\delta + 5\lambda^2 + 20\lambda^2\delta + (81 + 81\delta^2 + 430\lambda^2\delta + 162\delta + 300\lambda^2\delta^2 + 130\lambda^2 + 140\lambda^4\delta + 580\lambda^4\delta^2 - 15\lambda^4)^{1/2}]. \quad (124)$$

For  $\delta = 1$  and  $\lambda^2 = 3.61$ , expression (124) gives  $\beta_{c3} = 56.143$ , consistent with the upper curve in Fig. 25. There is no essential mathematical difficulty of obtaining a more general analytical form of  $\beta_{c3}$  for arbitrary values of  $\alpha$ , although the expression may appear somewhat complicated.

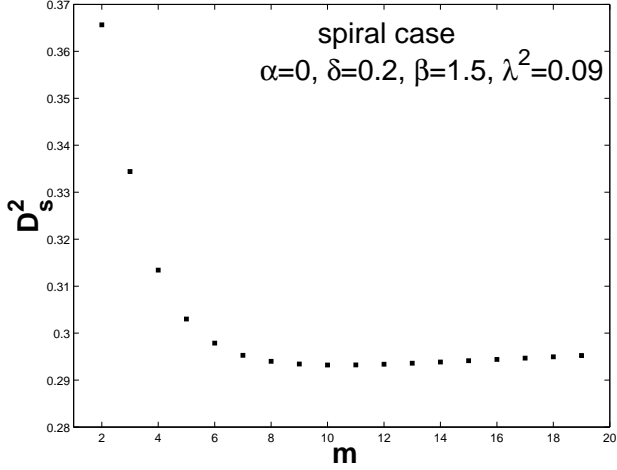


**Figure 27.** Solutions of  $D_s^2$  for the  $y_2$  branch versus  $|m|$  with parameters  $\alpha = 0$ ,  $\delta = 0.2$ ,  $\beta = 1.5$  and  $\lambda^2 = 0.09$ . The smallest  $D_s^2$  appears at  $|m| = 10$ .

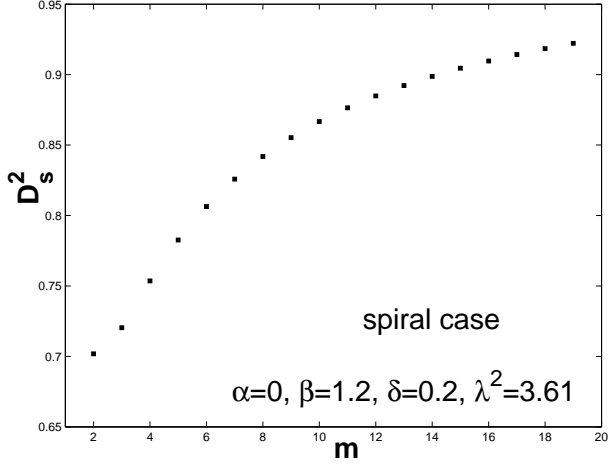


**Figure 28.** Solutions of  $D_s^2$  for the  $y_2$  branch versus  $|m|$  with parameters  $\alpha = 0$ ,  $\delta = 0.2$ ,  $\beta = 1.2$  and  $\lambda^2 = 3.61$ . The smallest  $D_s^2$  appears at  $|m| = 2$ .

Physically, one may exchange the role of  $|m|$  and  $\alpha$  as they both contribute to the total dimensionless wavenumber. Given a fixed  $\alpha$  value, a composite MSID system may support different values of  $|m|$  (see fig. 3 of Shu et al. 2000 and figs. 14 and 15 of Lou & Shen 2003). This is shown here in Figs. 27 and 28. Analogous to the aligned case, the smallest value of  $y_2 \equiv D_s^2$  occurs at an azimuthal periodicity of  $|m| = 10$  with parameters  $\alpha = 0$ ,  $\delta = 0.2$ ,  $\beta = 1.5$  and  $\lambda^2 = 0.09$ . As a comparison, for the same  $\delta = 0.2$  and  $\alpha = 0$  yet a smaller  $\beta = 1.2$  and a stronger magnetic field  $\lambda^2 = 3.61$ , the smallest value of  $y_2 \equiv D_s^2$  then occurs at  $|m| = 2$ . Again, we see that the stability of a composite (M)SID system appears to be more complicated than those of a single (M)SID system by the involvement of three parameters. As parameters  $\delta$ ,  $\beta$  and  $\lambda^2$  vary, vulnerable configurations with the smallest  $D_s^2$  value change accordingly.

## 5 DISCUSSION AND SUMMARY

In this final section we outline some potential applications of our analysis in the context of a nearby spiral galaxy NGC 6946, and then summarize our theoretical results and suggestions.

### 5.1 Galactic Applications

By the hydrodynamic density-wave scenario for a disc galaxy, large-scale high gas density spiral arms are vulnerable to molecular cloud and star formation activities on smaller scales and are therefore luminous in optical bands. As synchrotron radio observations also reveal large-scale spiral structures in association with optical spiral arms (e.g. Mathewson et al. 1972; Sofue et al. 1986; Beck et al. 1996), it is necessary to incorporate galactic magnetic field embedded in the interstellar medium (ISM) and an relativistic cosmic-ray gas (Lou & Fan 2003) in the MHD density-wave scenario for a deeper physical understanding (Fan & Lou 1996; Lou & Fan 1998a).

The interlacing of optical and magnetic spiral arms in the nearby spiral galaxy NGC 6946 was first revealed by Beck & Hoernes (1996) in the inner disc portion with an almost rigid rotation. Similar features of displaced optical and radio arms were also reported in portions of spiral galaxies IC 342 (e.g. Krause et al. 1989) and M83 (NGC 5236; e.g. Sukumar & Allen 1989; Neininger 1992; Neininger et al. 1993). These observational results led Fan & Lou (1996) to introduce theoretical concepts of slow MHD density waves (SMDWs) and fast MHD density waves (FMDWs) in magnetized spiral galaxies (Lou & Fan 1998a; Lou, Yuan & Fan 2001) and to show that perturbation enhancements of azimuthal magnetic field and gas mass density of SMDW are phase shifted by  $\gtrsim \pi/2$  relative to each other. However, several wavelet analysis on multi-wavelength data of NGC 6946 (e.g. Frick et al. 2000, 2001) further revealed large-scale spiral arms extended well into the outer disc portion with a more or less flat rotation curve (e.g. Tacconi & Young 1989; Sofue 1996; Ferguson et al. 1998), that seems to challenge earlier arguments that SMDWs are largely confined within the inner disc portion of almost rigid rotation.

For coplanar MHD perturbation structures of stationary logarithmic spirals in an MSID model with a flat rotation curve, Lou (2002) has shown the existence of SMDWs. For stationary SMDWs of Lou (2002), logarithmic spiral enhancements of gas surface mass density and azimuthal magnetic field are phase shifted by about  $\pi/2 \sim \pi$ . As effects of long-range self-gravity, magnetic field and disc differential rotation are included in the model analysis, SMDW patterns in a single MSID model can indeed support extended manifestations of interlaced optical and magnetic spiral arms that persist well into the outer disc portion with a flat rotation curve (Lou & Fan 2002). Moreover, Lou (2002) further suggested that significant phase shifts between  $0 \sim \pi/2$  related to stationary logarithmic spiral structures of FMDWs within a single MSID.

Given idealizations of our composite MSID model, the three possible stationary logarithmic spiral patterns might be conceptually relevant to magnetized spiral galaxies. Specifically, for the upper two solution branches of  $y_1$  and  $y_2$ , the phase difference of the stationary logarithmic spiral enhancements between azimuthal magnetic field and surface mass gas density is between  $\pi/2 \sim \pi$ , supporting the idea that interlaced optical and magnetic spiral arms may persist through the inner disc portion to the outer portion (with a phase difference  $\geq \pi/2$ ). For a sufficiently large  $\alpha$  in the tight-winding or WKBJ regime, this phase difference approaches  $\sim \pi$ , while for a sufficiently small  $\alpha$  in the open regime, this phase difference approaches  $\pi/2$ . Note that in our modelling, the phase difference of  $0 \sim \pi/2$  occurs mainly through the  $y_3$  solution branch that is usually unphysical with  $D_s^2$  being negative.

As sketched earlier (e.g. Lou & Fan 1998a, 2000a, b; Lou et al. 2002), a typical disc galaxy involves a stellar disc, a magnetized gas disc and a massive dark matter halo. Our theoretical model of a composite MSID system, idealized and simplified in many aspects, does contain these basic elements. With necessary qualifications in mind, it is then of considerable interest to reveal possible types of large-scale structures and their characteristic features in the stationary MHD density-wave scenario and relate them to galactic diagnostics and observations.

For the  $y_1$  solution with largest value of  $D_s^2$ , stationary logarithmic spiral density arms in gaseous MSID and in stellar SID are spatially out of phase; in particular, spiral gas density and magnetic field arms are significantly phase shifted relative to each other with a phase difference between  $\pi/2 \sim \pi$ .

For the  $y_2$  solution with middle value of  $D_s^2$ , stationary logarithmic spiral density arms in gaseous MSID and in stellar SID are spatially in phase; meanwhile, spiral gas density and magnetic field arms are significantly phase shifted relative to each other with a phase difference between  $\pi/2 \sim \pi$  for  $\beta > 1$  and  $\beta > \beta_{c0}$ . At the qualitative level, this case appears comparable to interlaced optical and synchrotron radio arms of NGC 6946 (Beck & Hoernes 1996; Fan & Lou 1996; Frick et al. 2000, 2001; Lou & Fan 2002). On the other hand, for  $1 < \beta < \beta_{c0}$ , stationary logarithmic spiral density arms in gaseous MSID and in stellar SID are spatially out of phase; meanwhile, spiral gas density and magnetic field arms are phase shifted relative to each other with a phase difference between  $0 \sim \pi/2$ .

By the above analogy of unaligned spiral configurations, our results for aligned stationary MHD perturbations with  $|m| = 2$  may bear possible diagnostics for optical and synchrotron radio observations of galactic bar structures and their spatial phase relationships. It is straightforward to compare Figs. 4–7 of the aligned cases with Figs. 21–24 and infer spatial phase relationships of stellar bars, gas bars and synchrotron radio bars involving magnetic fields. For example, by Figs. 4 and 6, the  $y_1$  solution describes a configuration in which the stellar density bar and the gas density bar are phase shifted relative to each other with a  $\pi$  phase

difference, while the gas density bar and the synchrotron radio bar (i.e. magnetic bar) are phase shifted relative to each other with a  $\pi$  phase difference. The  $y_2$  solution describes a configuration in which the stellar density bar and the gas density bar coincide, while the gas density bar and the synchrotron radio bar (i.e. magnetic bar) are phase shifted relative to each other with a  $\pi$  phase difference. By Figs. 5 and 7, the  $y_1$  solution describes a qualitatively similar bar configuration as the  $y_1$  configuration of Figs. 4 and 6. For  $\beta > \beta_{c0}$  [see definition (77) for  $\beta_{c0}$ ], the  $y_2$  solution describes a qualitatively similar bar configuration as the  $y_2$  configuration of Figs. 4 and 6. For  $1 < \beta < \beta_{c0}$ , the  $y_2$  solution describes a configuration in which the stellar density bar and the gas density bar are phase shifted relative to each other with a  $\pi$  phase difference, while the gas density bar and the synchrotron radio bar (i.e. magnetic bar) coincide. In context of observations, the prominent bar structure of the nearby barred spiral galaxy M83 (e.g. Sukumar & Allen 1989; Neininger 1992; Neininger et al. 1993) is worth being analyzed in more details in both optical and synchrotron radio bands.

## 5.2 Summary

In terms of theoretical development of MSID model and in reference to previous theoretical analyses of Shu et al. (2000) on zero-frequency (i.e. stationary) aligned and unaligned perturbation configurations of an isopedically magnetized SID, of Lou (2002) on stationary aligned and unaligned perturbation configurations of a coplanarly magnetized SID, and of Lou & Shen (2003) on stationary aligned and unaligned perturbation structures in a composite system of two-fluid SIDs, we have constructed analytically in this paper stationary aligned and unaligned perturbation configurations in either full or partial composite system consisting of a stellar SID and a gaseous MSID. While this composite model of one SID and one MSID is highly idealized in many aspects, it does contain several necessary and more realistic elements that are pertinent to structures and dynamics of disc galaxies. Galactic structures may not be stationary in general, yet the stationary global MHD perturbation structures might represent a subclass, provide insights for a disc galaxy, and serve as benchmarks for numerical MHD simulations. Given our model specifications, we have reached the following conclusions and suggestions.

For aligned MHD perturbation structures, we derived stationary dispersion relation (62) for both full and partial composite system of one SID and one MSID. Mathematically, there are three possible  $D_s^2$  values for the square of dimensionless rotation parameter  $D_s$  of the stellar SID (or equivalently,  $D_g^2$ ). Physically, only those solutions with  $D_s^2 > 0$  and  $D_g^2 > 0$  may be conceptually applicable.

In the aligned case of barred configurations with  $|m| = 2$  and  $F = 1$  for a full composite MSID system, the uppermost branch remains always physically possible, with spatial phase relationships  $\mu_g/\mu_s < 0$  and  $\mu_g/Z < 0$  (where  $Z$  is the amplitude of azimuthal magnetic field perturbation);

that is, both  $\mu_g$  and  $\mu_s$  pair and  $\mu_g$  and  $Z$  pair are out of phase. These qualitative features for possible bars may be detectable observationally. When parameter  $\beta$  is smaller than a critical value  $\beta_{c1}$  defined by (71), the middle solution branch of  $y \equiv D_s^2$  is positive and thus physically possible. Corresponding phase relationships of  $\mu_g/\mu_s$  and of  $\mu_g/Z$  are in phase and out of phase, respectively. But when  $\beta < \beta_{c0}$  defined by expression (77),  $\mu_g/\mu_s$  and of  $\mu_g/Z$  can become zero or even change to opposite sign (see Figs. 5 and 7). This special  $\mu_g = 0$  case might be an additional possibility. The lowest branch of  $y \equiv D_s^2$  is physically possible only when  $\beta < \beta_{c2}$  defined by expression (72). In many cases  $\beta_{c2}$  is smaller than 1, this branch is thus invalid. However in some cases (see Fig. 2), this branch can rise up to become positive and thus physically possible. The corresponding phase relationships of  $\mu_g/\mu_s$  and  $\mu_g/Z$  are both always positive and thus in phase.

For aligned perturbations, the case of  $|m| = 0$  can be made to effectively rescale the axisymmetric background. Eccentric  $|m| = 1$  displacements may occur for arbitrary  $D_s^2$  values in a full composite MSID system. In contrast, for a partial composite MSID system,  $D_s^2$  can no longer be arbitrary for  $|m| = 1$  (Lou 2002; Lou & Shen 2003).

For coplanar MHD perturbation structures of unaligned logarithmic spirals, we obtained the stationary dispersion relation (106) for both full and partial composite MSID system. Mathematically, there are three possible sets of solutions for  $D_s^2$  or equivalently  $D_g^2$ .

For stationary logarithmic spiral configurations with  $|m| = 2$  and  $F = 1$  in a full composite MSID system, the uppermost  $D_s^2$  solution branch is always physically possible, with corresponding  $\mu_g/\mu_s$  being always out of phase and with the phase difference between  $\mu_g$  and  $Z$  in the range  $\pi/2 \sim \pi$ . The middle branch of  $D_s^2$  solution is physically possible when  $\beta < \beta_{c1}$  defined by expression (119). There also exists a special  $\beta_{c0}$  defined by expression (123); when  $\beta$  decreases below  $\beta_{c0}$ , the corresponding  $\mu_g/\mu_s$  changes from being in phase to being out of phase (see Fig. 22), and the phase difference between  $\mu_g$  and  $Z$  changes from being within  $\pi/2 \sim \pi$  to being within  $0 \sim \pi/2$  (see Fig. 24). The special  $\mu_g = 0$  case may occur as well. The lowest branch of  $D_s^2$  solution can be physically possible when  $\beta < \beta_{c2}$  defined by expression (120). Similar to the aligned case, while this lowest  $D_s^2$  solution branch is often invalid as  $\beta_{c2}$  is usually less than 1, it may become physically possible for  $\beta$  within interval  $[1, \beta_{c2}]$  (see Figs. 19 and 20) for cases with  $\beta_{c2} > 1$ . Correspondingly,  $\mu_g/\mu_s$  remains always in phase and the phase difference between  $\mu_g$  and  $Z$  falls in the range  $0 \sim \pi/2$ .

For the marginal case of  $|m| = 0$  with radial propagations, the collapse and ring fragmentation regimes exist, while the lower ring fragmentation curve, which is a novel feature in a single MSID (Lou 2002), does not often appear to be positive. For cases with  $\beta \simeq 1$ , this lower ring fragmentation branch may rise to become positive and will descend with increasing  $\lambda^2$  as shown in Figs. 15 and 16. This qualitative trend differs from that of a single MSID

studied by Lou (2002). We further examined trends of variation as parameters  $\delta$ ,  $\beta$  and  $\lambda^2$  vary, and concluded that the mutual gravitational coupling between the two SIDs appears to reduce collapse regime but to increase the danger of ring fragmentation. Physical interpretations on collapse and ring fragmentation regimes are provided (Shu et al. 2000; Lou 2002; Lou & Shen 2003; Shen & Lou 2003). Consistent with prior analyses, we realize that the ring fragmentation curve has a fixed vertical asymptote at  $\mathcal{N}_0(\alpha)(\alpha^2 + 1/4) = 2$  with  $\alpha \sim 1.759$  approximately; this condition for the vertical asymptote remains exactly the same as that of Shu et al. (2000), Lou (2002) and Lou & Shen (2003). In reference to these previous analyses, it is highly suggestive that the effective  $Q$  parameter in a composite MSID system should be closely related to the minimum of the ring fragmentation curve (Shen & Lou 2003).

The unaligned spiral case of  $|m| = 1$  is somewhat special. Being negative, the two lower solution branches of  $D_s^2$  are both unphysical. The uppermost  $D_s^2$  solution branch is physically possible when  $\beta < \beta_{c3}$ . The analytic expression of  $\beta_{c3}$  with  $\alpha = 1$  is given by equation (124).

We have also derived the MHD virial theorem in a composite MSID system, following the suggestion of Lou (2002) that ratio  $\mathcal{T}/|\mathcal{W} - \mathcal{M}|$  may play the role of ratio  $\mathcal{T}/|\mathcal{W}|$  in determining the onset criterion for bar-like instability when coplanar magnetic field is involved. Similar to a composite system of two fluid SIDs of Lou & Shen (2003), we found that solution  $D_s^2$  of the middle  $y_2$  branch may correspond to  $\mathcal{T}/|\mathcal{W} - \mathcal{M}|$  ratios being considerably lower than the oft-quoted value of  $\sim 0.14$  (Ostriker & Peebles 1973; Binney & Tremaine 1987). This indicates that a composite (M)SID system tends to be less stable. This is just one perspective of showing that the stability in a composite MSID system is far more complicated than that of a single MSID. In particular, additional solution branches allowed by more dynamic freedoms as well as more parameters  $\delta$ ,  $\beta$  and  $\lambda^2$  do introduce extra dimensions for the stability problems. For example, as these dimensionless parameters vary, most vulnerable configurations related to the smallest  $D_s^2$  change.

While our model for a composite system of MSIDs is highly idealized, theoretical results obtained here provide a conceptual basis and useful clues for optical and synchrotron radio observational diagnostics of spiral galaxies of stars and gaseous ISM with magnetic field coupled by mutual gravity on large scales. In particular, our analytical solutions for stationary MHD perturbation configurations in a composite MSID system as well as analytical expressions for critical points are important and valuable for benchmarking numerical codes designed for large-scale dynamics of magnetized gaseous discs.

## ACKNOWLEDGMENTS

This research was supported in part by the ASCI Center for Astrophysical Thermonuclear Flashes at the University of Chicago under Department of Energy contract B341495, by

the Special Funds for Major State Basic Science Research Projects of China, by the Tsinghua Center for Astrophysics, by the Collaborative Research Fund from the National Natural Science Foundation of China (NSFC) for Young Outstanding Overseas Chinese Scholars (NSFC 10028306) at the National Astronomical Observatory, Chinese Academy of Sciences, by NSFC grant 10373009 at the Tsinghua University, and by the Yangtze Endowment from the Ministry of Education through the Tsinghua University. Affiliated institutions of Y.Q.L. share the contribution.

## REFERENCES

- Beck R., Hoernes P., 1996, *Nat*, 379, 47  
 Beck R., et al. 1996, *ARA&A*, 34, 155  
 Bertin G., Romeo A.B., 1988, *A&A*, 195, 105  
 Binney J., Tremaine S., 1987, *Galactic Dynamics*. Princeton University Press, Princeton, New Jersey  
 Chakrabarti S., Laughlin G., Shu F. H., 2003, *ApJ*, in press,  
 Elmegreen B.G., 1995, *MNRAS*, 275, 944  
 Fan Z.H., Lou Y.-Q., 1996, *Nat*, 383, 800  
 Fan Z.H., Lou Y.-Q., 1997, *MNRAS*, 291, 91  
 Fan Z.H., Lou Y.-Q., 1999, *MNRAS*, 307, 645  
 Ferguson A.M.N., Wyse R.F.G., Gallagher J.S., Hunter D.A., 1998, *ApJ*, 506, L19  
 Frick P., Beck R., Shukurov A., Sokoloff D., Ehle M., Kamphuis J., 2000, *MNRAS*, 318, 925  
 Frick P., Beck R., Berkhuijsen E.M., Patrickeyev I., 2001, *MNRAS*, 327, 1145  
 Galli D., Shu F.H., Laughlin G., Lizano S., 2001, *ApJ*, 551, 367  
 Goodman J., Evans N.W., 1999, *MNRAS*, 309, 599  
 Hohl F., 1971, *ApJ*, 168, 343  
 Jog C.J., 1996, *MNRAS*, 278, 209  
 Jog C.J., Solomon P.M., 1984a, *ApJ*, 276, 114  
 Jog C.J., Solomon P.M., 1984b, *ApJ*, 276, 127  
 Kalnajs A.J., 1971, *ApJ*, 166, 275  
 Kalnajs A.J., 1972, *ApJ*, 175, 63  
 Kalnajs A.J., 1973, *Proc. Astron. Soc. Australia*, 2, 174  
 Kato S., 1972, *PASJ*, 24, 61  
 Kennicutt R.C., Jr, 1989, *ApJ*, 344, 685  
 Krause M., Hummel E., Beck R., 1989, *A&A*, 217, 4  
 Lemos J.P.S., Kalnajs A.J., Lynden-Bell D., 1991, *ApJ*, 375, 484  
 Lin C.C., Shu F.H., 1964, *ApJ*, 140, 646  
 Lin C.C., Shu F.H., 1966, *Proc. Natl Acad. Sci., USA*, 73, 3758  
 Lin C.C., Shu F.H., 1968, in Chrétián M., Deser S., Goldstein J., eds, *Summer Institute in Theoretical Physics*, Brandeis Univ., Astrophysics and General relativity. Gordon and Breach, New York, p.239  
 Lou Y.-Q., 2002, *MNRAS*, 337, 225  
 Lou Y.-Q., Fan Z.H., 1998a, *ApJ*, 493, 102  
 Lou Y.-Q., Fan Z.H., 1998b, *MNRAS*, 297, 84  
 Lou Y.-Q., Fan Z.H., 2000a, *MNRAS*, 315, 646  
 Lou Y.-Q., Fan Z.H., 2000b, in Berkhuijsen E.M., Beck R., Wal-  
 terbos R.A.M., eds, *The Interstellar Medium in M31 and M33*.  
 232 WE-Heraeus Seminar. Shaker Verlag, Aachen, 205  
 Lou Y.-Q., Fan Z.H., 2002, *MNRAS*, 329, L62  
 Lou Y.-Q., Fan Z.H., 2003, *MNRAS*, 341, 909  
 Lou Y.-Q., Shen Y., 2003, *MNRAS*, 343, 750  
 Lou Y.-Q., Yuan C., Fan Z.H., 2001, *ApJ*, 552, 189  
 Lou Y.-Q., Walsh W.M., Han J.L., Fan Z.H., 2002, *ApJ*, 567, 289  
 Lowe S.A., Roberts W.W., Jr, Yang J., Bertin G., Lin C.C., 1994,  
*ApJ*, 427, 184  
 Lynden-Bell D., Lemos J. P.S., 1993, *astro-ph/9907093*  
 Mathewson D.S., van der Kruit P.C., Brouw W.N., 1972, *A&A*,  
 17, 468  
 Mestel L., 1963, *MNRAS*, 157, 1  
 Miller R.H., Prendergast K.H., Quirk W.J., 1970, *ApJ*, 161, 903  
 Neininger N., 1992, *A&A*, 263, 30  
 Neininger N., Beck R., Sukumar S., Allen R.J., 1993, *A&A*, 274,  
 687  
 Ostriker J.P., 1978, in Lebovitz N.R., Reid W.H., Vandervoort  
 P.O., eds, *Theoretical principles in Astrophysics and Relativ-*  
*ity*. Univ. Chicago Press, Chicago. p.59  
 Ostriker J.P., Peebles P.J.E., 1973, *ApJ*, 186, 467  
 Romeo A.B., 1992, *MNRAS*, 256, 307  
 Safronov V.S., 1960, *Ann. Astrophys.*, 23, 979  
 Shen Y., Lou Y.-Q., 2003, *MNRAS*, in press, *astro-ph/0308063*  
 Shu F.H., Laughlin G., Lizano S., Galli D., 2000, *APJ*, 535, 190  
 Sofue Y., 1996, *ApJ*, 458, 120  
 Sofue Y., Fujimoto M., Wielebinski R., 1986, *ARA&A*, 24, 459  
 Sukumar S., Allen R.J., 1989, *Nat*, 340, 537  
 Syer D., Tremaine S., 1996, *MNRAS*, 281, 925  
 Tacconi L.J., Young J.S., 1989, *ApJS*, 71, 455  
 Toomre A., 1964, *ApJ*, 139, 1217  
 Toomre A., 1977, *ARA&A*, 15, 437  
 Vandervoort P.O., 1991a, *ApJ*, 377, 49  
 Vandervoort P.O., 1991b, *ApJ*, 383, 498  
 Wang B., Silk J., 1994, *ApJ*, 427, 759  
 Zang T.A., 1976, PhD Thesis, MIT, Cambridge MA

## APPENDIX A:

For the spiral case of  $|m| = 2$ , a substitution of expressions (11), (14), (19), (20) and (23) into equation (106) would lead to a cubic algebraic equation in terms of  $y \equiv D_s^2$ . By setting the constant term of this cubic equation equal to zero, we derive conditions for  $y = 0$ , namely

$$\mathcal{A}\beta^2 + \mathcal{B}\beta + \mathcal{C} = 0, \quad (\text{A1})$$

where the three coefficients  $\mathcal{A}$ ,  $\mathcal{B}$  and  $\mathcal{C}$  are defined by

$$\begin{aligned} \mathcal{A} \equiv & -578\mathcal{N}_2(\alpha)\delta - 32\alpha^4\mathcal{N}_2(\alpha)\delta - 272\mathcal{N}_2(\alpha)\delta\alpha^2 \\ & + 272\mathcal{N}_2(\alpha) + 64\alpha^2\mathcal{N}_2(\alpha) - 272 - 64\alpha^2 \\ & - 64\delta\alpha^2 - 272\delta, \end{aligned} \quad (\text{A2})$$

$$\begin{aligned} \mathcal{B} \equiv & -400\alpha^2\mathcal{N}_2(\alpha) + 272\mathcal{N}_2(\alpha)\delta\alpha^2 + 32\alpha^4 \\ & + 32\alpha^4\mathcal{N}_2(\alpha)\delta + 32\alpha^4\lambda^2 + 578\mathcal{N}_2(\alpha)\delta - 34\mathcal{N}_2(\alpha)\lambda^2 \\ & - 1122\mathcal{N}_2(\alpha) + 400\alpha^2 + 1122 + 144\delta\lambda^2\alpha^2 + 32\alpha^4\delta\lambda^2 \\ & + 34\delta\lambda^2 - 144\mathcal{N}_2(\alpha)\lambda^2\alpha^2 + 34\lambda^2 - 32\alpha^4\mathcal{N}_2(\alpha) + 1122\delta \\ & + 16\alpha^4\mathcal{N}_2(\alpha)\delta\lambda^2 + 400\delta\alpha^2 + 32\alpha^4\delta + 144\lambda^2\alpha^2 \\ & + 120\mathcal{N}_2(\alpha)\delta\lambda^2\alpha^2 + 221\mathcal{N}_2(\alpha)\delta\lambda^2 - 32\alpha^4\mathcal{N}_2(\alpha)\lambda^2 \end{aligned} \quad (\text{A3})$$

and

$$\begin{aligned} \mathcal{C} \equiv & -850 - 264\lambda^2\alpha^2 - 264\delta\lambda^2\alpha^2 - 32\alpha^4 + 96\lambda^4\delta\alpha^2 \\ & + 96\lambda^4\alpha^2 + 16\alpha^4\lambda^4\delta - 48\alpha^4\delta\lambda^2 - 850\delta - 32\alpha^4\delta \\ & + 16\lambda^4\alpha^4 - 336\alpha^2 - 255\lambda^2 - 255\delta\lambda^2 \\ & - 336\delta\alpha^2 + 119\lambda^4\delta + 119\lambda^4 - 48\alpha^4\lambda^2 \\ & + 850\mathcal{N}_2(\alpha) + 264\mathcal{N}_2(\alpha)\lambda^2\alpha^2 - 96\lambda^4\mathcal{N}_2(\alpha)\alpha^2 \\ & + 255\mathcal{N}_2(\alpha)\lambda^2 - 119\lambda^4\mathcal{N}_2(\alpha) + 336\alpha^2\mathcal{N}_2(\alpha) \\ & + 32\alpha^4\mathcal{N}_2(\alpha) - 16\alpha^4\lambda^4\mathcal{N}_2(\alpha) + 48\alpha^4\mathcal{N}_2(\alpha)\lambda^2. \end{aligned} \quad (\text{A4})$$

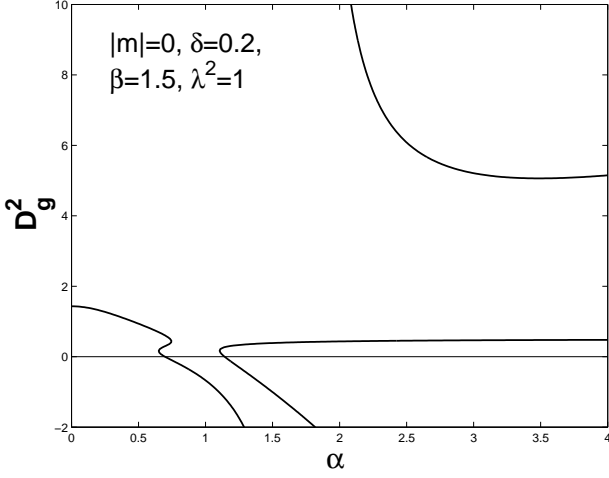


**Figure B1.** The marginal stability curve of  $D_g^2$  versus  $\alpha$  with parameters  $|m| = 0$ ,  $\delta = 0.2$ ,  $\beta = 1.5$  and  $\lambda^2 = 1$ . Fig. B2 presents corresponding curves of  $D_s^2$  versus  $\alpha$ .

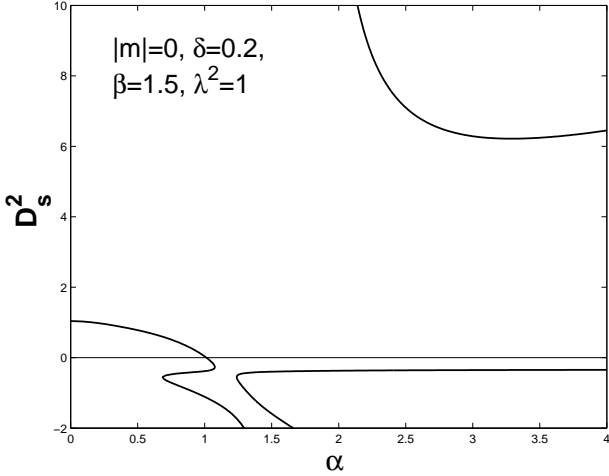


**Figure B2.** The marginal stability curve of  $D_s^2$  versus  $\alpha$  with parameters  $|m| = 0$ ,  $\delta = 0.2$ ,  $\beta = 1.5$ ,  $\lambda^2 = 1$ . Fig. B1 presents corresponding curves of  $D_g^2$  versus  $\alpha$ .

## APPENDIX B:

In the presence of gravitational coupling between one SID and one MSID, we expect three sets of independent mathematical solutions in general. However, for cases of marginal stabilities for spiral configurations with  $|m| = 0$ , the solution curves qualitatively resemble those determined for a single SID (Shu et al. 2000) in most cases, and the two extra solutions turn out to be negative. Moreover, the lower ring fragmentation curve in a single MSID (see fig. 1 of Lou 2002) remains often indiscernible (see Figs. 11–15). Here, we provide a complete structure for solution curves in Figs. B1 and B2.

We note that the basic positive  $D_g^2$  versus  $\alpha$  profile is qualitatively similar to fig. 1 of Lou (2002) (see Fig. B1). However, the  $D_s^2$  curve corresponding to the lower ring fragmentation curve of  $D_g^2$  is negative in most cases, indicating

that this branch is physically invalid (see Figs. B1 and B2). On the other hand, when  $\beta$  approaches 1, this branch of  $D_s^2$  can be raised above zero and thus becomes physically valid in this limit (see Fig. 15).

## APPENDIX C:

In this Appendix C, we provide the complete form of the cubic equation of  $y \equiv D_s^2$  for the aligned case of coplanar MHD perturbations in a composite MSID system for interested readers or potential users in numerical MHD simulations. From dispersion relation (62) and relation (23), we readily derive

$$\mathcal{A}y^3 + \mathcal{B}y^2 + \mathcal{C}y + \mathcal{D} = 0, \quad (\text{C1})$$

where the four coefficients  $\mathcal{A}$ ,  $\mathcal{B}$ ,  $\mathcal{C}$  and  $\mathcal{D}$  are defined by

$$\begin{aligned} \mathcal{A} \equiv & -16|m|\beta^2 - 4m^4\beta^2(1+\delta) + 16m^2|m|\beta^2 \\ & -4m^4|m|\beta^2 - 16|m|\delta\beta^2 + 8m^2\delta\beta^2 \\ & -4m^4|m|\delta\beta^2 + 8m^2\beta^2 + 16m^2|m|\delta\beta^2, \end{aligned} \quad (\text{C2})$$

$$\begin{aligned} \mathcal{B} \equiv & -4m^4\delta\beta^2 - 16m^2\beta - 4m^4|m|\beta^2 + 2m^4\delta\lambda^2\beta \\ & -32|m|\beta^2 + 32|m|\delta\beta - 4m^4|m|\delta\beta^2 \\ & +32|m|\beta - 40m^2|m|\delta\beta + 4m^4\delta\beta + 16m^2\delta\beta^2 \\ & +24m^2\beta^2 + 24m^2|m|\beta^2 - 32|m|\delta\beta^2 \\ & +12m^4|m|\delta\beta - 8m^2\delta\beta - 12m^4\beta^2 \\ & +4\delta\lambda^2\beta + 12m^4\beta + 24m^2|m|\delta\beta^2 \\ & -6m^2\delta\lambda^2\beta + 12m^4|m|\beta - 40m^2|m|\beta, \end{aligned} \quad (\text{C3})$$

$$\begin{aligned} \mathcal{C} \equiv & 24m^2|m|\delta + 2\lambda^2m^2 - 8m^4 + 24m^2|m| + m^4\lambda^4 \\ & -\lambda^4m^2 - 16|m|\delta + m^4\lambda^4|m| - 32m^2\beta + 24m^2\beta^2 \\ & -8m^4|m| - 16|m| + 6m^2\lambda^2|m|\delta - 2m^4\lambda^2|m|\delta \\ & -3|m|\lambda^4m^2\delta + 6m^2\lambda^2|m| - 3m^2\lambda^4|m| \\ & -2m^4\lambda^2|m| - 2m^4\lambda^2 - 4|m|\lambda^2 - 4|m|\delta\lambda^2 \\ & -4m^2\delta\lambda^2\beta - 8m^2\delta\beta + 4m^4\delta\beta^2 + 8m^2\delta\beta^2 \\ & -8m^4|m|\delta + 8m^2 - 24m^2|m|\beta + 24m^4\beta \\ & -12m^4\beta^2 + 4m^4|m|\beta^2 - 24m^2|m|\delta\beta + m^4\lambda^4|m|\delta \\ & +4m^4|m|\delta\beta^2 + 4\delta\lambda^2\beta - 16|m|\beta^2 + 32|m|\beta \\ & +2\lambda^4|m| - 16|m|\delta\beta^2 + 32|m|\delta\beta + 2\lambda^4|m|\delta \end{aligned} \quad (\text{C4})$$

and

$$\begin{aligned} \mathcal{D} \equiv & -8m^2|m|\delta + 2\lambda^2m^2 - 8m^4 - 8m^2|m| + m^4\lambda^4 \\ & -\lambda^4m^2 - m^4\lambda^4|m| - 16m^2\beta + 8m^2\beta^2 + 8m^4|m| \\ & -2m^2\lambda^2|m|\delta + 2m^4\lambda^2|m|\delta + |m|\lambda^4m^2\delta - 2m^2\lambda^2|m| \\ & +m^2\lambda^4|m| + 2m^4\lambda^2|m| - 2m^4\lambda^2 - 4m^4\delta\beta + 2m^2\delta\lambda^2\beta \\ & -2m^4\delta\lambda^2\beta + 4m^4\delta\beta^2 + 8m^4|m|\delta + 8m^2 - 8m^2|m|\beta^2 \\ & +16m^2|m|\beta + 12m^4\beta - 12m^4|m|\beta - 4m^4\beta^2 \\ & +4m^4|m|\beta^2 - 12m^4|m|\delta\beta + 16m^2|m|\delta\beta \\ & -m^4\lambda^4|m|\delta - 8m^2|m|\delta\beta^2 + 4m^4|m|\delta\beta^2. \end{aligned} \quad (\text{C5})$$

One can solve cubic equation (C1) for possible aligned MHD perturbation configurations in a composite MSID system by specifying parameters  $m$ ,  $\delta$ ,  $\beta$  and  $\lambda$ .

#### APPENDIX D:

In this Appendix D, we provide the complete form of the cubic equation of  $y \equiv D_s^2$  for the unaligned spiral case of coplanar MHD perturbations in a composite MSID system for interested readers or potential users in numerical MHD simulations. From dispersion relation (62) and relation (23), we readily derive

$$\mathcal{A}y^3 + \mathcal{B}y^2 + \mathcal{C}y + \mathcal{D} = 0, \quad (\text{D1})$$

where the four coefficients  $\mathcal{A}$ ,  $\mathcal{B}$ ,  $\mathcal{C}$  and  $\mathcal{D}$  are defined by

$$\begin{aligned} \mathcal{A} \equiv & 32m^2\mathcal{N}_m(\alpha)\alpha^2\beta^2 + 32m^2\mathcal{N}_m(\alpha)\delta\alpha^2\beta^2 \\ & -16\mathcal{N}_m(\alpha)\beta^2 + 128\delta\beta^2 - 128m^2\beta^2 + 32m^4\beta^2 + 128\beta^2 \\ & -16\mathcal{N}_m(\alpha)\delta\beta^2 - 64\mathcal{N}_m(\alpha)\alpha^2\beta^2 - 56\mathcal{N}_m(\alpha)m^2\beta^2 \\ & +32m^4\mathcal{N}_m(\alpha)\beta^2 - 64\mathcal{N}_m(\alpha)\delta\alpha^2\beta^2 + 32m^4\mathcal{N}_m(\alpha)\delta\beta^2 \\ & -56\mathcal{N}_m(\alpha)\delta m^2\beta^2 + 32m^4\delta\beta^2 - 128m^2\delta\beta^2, \end{aligned} \quad (\text{D2})$$

$$\begin{aligned} \mathcal{B} \equiv & -16m^4\mathcal{N}_m(\alpha)\delta\lambda^2\beta - 16m^2\mathcal{N}_m(\alpha)\delta\lambda^2\alpha^2\beta \\ & -32m^2\mathcal{N}_m(\alpha)\lambda^2\alpha^2\beta \\ & +30\mathcal{N}_m(\alpha)\beta - 128m^2\mathcal{N}_m(\alpha)\alpha^2\beta + 64\mathcal{N}_m(\alpha)\delta\alpha^2\beta \\ & -32m^4\mathcal{N}_m(\alpha)\delta\beta - 32m^2\mathcal{N}_m(\alpha)\delta\alpha^2\beta - 32m^2\alpha^2\delta\beta \\ & +56\mathcal{N}_m(\alpha)\delta m^2\beta + 64\alpha^2\beta - 240\delta\beta \\ & -96m^4\beta + 96\mathcal{N}_m(\alpha)m^2\beta + 112\mathcal{N}_m(\alpha)\alpha^2\beta \\ & +64\alpha^2\delta\beta - 32m^2\alpha^2\beta - 96m^4\mathcal{N}_m(\alpha)\beta \\ & +16\mathcal{N}_m(\alpha)\delta\beta + 16\lambda^2\beta - 32m^2\delta\lambda^2\alpha^2\beta \\ & +64\delta\lambda^2\alpha^2\beta - 24\mathcal{N}_m(\alpha)\delta\lambda^2\beta - 32m^2\lambda^2\alpha^2\beta \\ & -8\mathcal{N}_m(\alpha)\lambda^2m^2\beta - 16\mathcal{N}_m(\alpha)\lambda^2\alpha^2\beta - 32\alpha^4\mathcal{N}_m(\alpha)\lambda^2\beta \\ & -2\mathcal{N}_m(\alpha)\lambda^2\beta + 64\lambda^2\alpha^2\beta - 8\lambda^2m^2\beta \\ & -32\alpha^4\mathcal{N}_m(\alpha)\beta + 32\mathcal{N}_m(\alpha)\delta\alpha^2\beta\lambda^2 + 44\mathcal{N}_m(\alpha)\delta m^2\beta\lambda^2 \\ & -144\mathcal{N}_m(\alpha)\delta\alpha^2\beta^2 - 128\mathcal{N}_m(\alpha)\delta m^2\beta^2 - 32m^2\alpha^2\delta\beta^2 \\ & +96m^2\mathcal{N}_m(\alpha)\alpha^2\beta^2 + 32m^4\beta^2 - 48\mathcal{N}_m(\alpha)\beta^2 + 64\alpha^2\beta^2 \\ & +272\delta\beta^2 - 168\mathcal{N}_m(\alpha)m^2\beta^2 - 192\mathcal{N}_m(\alpha)\alpha^2\beta^2 \\ & +64\alpha^2\delta\beta^2 - 32m^2\alpha^2\beta^2 + 96m^4\mathcal{N}_m(\alpha)\beta^2 \\ & -34\mathcal{N}_m(\alpha)\delta\beta^2 + 32m^4\mathcal{N}_m(\alpha)\delta\beta^2 - 32\alpha^4\mathcal{N}_m(\alpha)\delta\beta^2 \\ & -200m^2\beta^2 - 240\beta + 272\beta^2 \\ & -96m^4\delta\beta - 8m^2\delta\lambda^2\beta + 312m^2\delta\beta \\ & +32m^4\delta\beta^2 - 200m^2\delta\beta^2 + 312m^2\beta + 16\delta\lambda^2\beta, \end{aligned} \quad (\text{D3})$$

$$\begin{aligned} \mathcal{C} \equiv & 112 - 96\delta\lambda^2\alpha^2 - \mathcal{N}_m(\alpha)\lambda^2 + \lambda^4\mathcal{N}_m(\alpha) \\ & +16m^4\lambda^2 - 36m^2\delta\lambda^2 + 20\lambda^4m^2\delta \\ & +48m^2\lambda^2\alpha^2 + 8\delta\lambda^2 - 8m^4\lambda^4\delta \\ & +16m^4\delta\lambda^2 + 20m^2\lambda^4 + 16m^4\mathcal{N}_m(\alpha)\lambda^2 \\ & +8\mathcal{N}_m(\alpha)\lambda^2\alpha^2 - 64\alpha^2 - 96\lambda^2\alpha^2 \\ & -40m^2\mathcal{N}_m(\alpha) - 64\alpha^2\delta - 48\alpha^2\mathcal{N}_m(\alpha) \\ & +32\alpha^2\lambda^4 + 2\lambda^4\mathcal{N}_m(\alpha)m^2 - 8\lambda^4\delta \\ & +16m^2\mathcal{N}_m(\alpha)\delta\lambda^2\alpha^2\beta - 16m^2\lambda^4\delta\alpha^2 - 24m^2\lambda^4\mathcal{N}_m(\alpha)\alpha^2 \\ & +48m^2\delta\lambda^2\alpha^2 + 32m^2\alpha^2 + 32m^2\alpha^2\delta \\ & -8m^4\lambda^4 + 64m^2\mathcal{N}_m(\alpha)\lambda^2\alpha^2 - 64m^2\mathcal{N}_m(\alpha)\lambda^2\alpha^2\beta \\ & +16\alpha^4\mathcal{N}_m(\alpha)\delta\lambda^2\beta + 60\mathcal{N}_m(\alpha)\beta - 256m^2\mathcal{N}_m(\alpha)\alpha^2\beta \\ & +80\mathcal{N}_m(\alpha)\delta\alpha^2\beta + 32\alpha^4\mathcal{N}_m(\alpha)\delta\beta + 32m^2\mathcal{N}_m(\alpha)\delta\alpha^2\beta \\ & +96m^2\alpha^2\delta\beta + 72\mathcal{N}_m(\alpha)\delta m^2\beta - 48\alpha^2\beta \\ & -270\delta\beta + 192\mathcal{N}_m(\alpha)m^2\beta + 224\mathcal{N}_m(\alpha)\alpha^2\beta \\ & -48\alpha^2\delta\beta + 96m^2\alpha^2\beta - 192m^4\mathcal{N}_m(\alpha)\beta \\ & +18\mathcal{N}_m(\alpha)\delta\beta + 32\alpha^2\lambda^4\delta + 18\lambda^2\beta \\ & +80\delta\lambda^2\alpha^2\beta - 27\mathcal{N}_m(\alpha)\delta\lambda^2\beta + 32\alpha^4\delta\lambda^2\beta \\ & -16\mathcal{N}_m(\alpha)\lambda^2m^2\beta - 32\mathcal{N}_m(\alpha)\lambda^2\alpha^2\beta - 64\alpha^4\mathcal{N}_m(\alpha)\lambda^2\beta \\ & -4\mathcal{N}_m(\alpha)\lambda^2\beta + 80\lambda^2\alpha^2\beta + 32\alpha^4\lambda^2\beta \\ & +112\delta + 32\alpha^4\beta + 32\alpha^4\delta\beta \\ & -64\alpha^4\mathcal{N}_m(\alpha)\beta + 24\mathcal{N}_m(\alpha)\delta\alpha^2\beta\lambda^2 - 96m^2\mathcal{N}_m(\alpha)\delta\alpha^2\beta^2 \\ & +36\mathcal{N}_m(\alpha)\delta m^2\beta\lambda^2 - 96\mathcal{N}_m(\alpha)\delta\alpha^2\beta^2 - 88\mathcal{N}_m(\alpha)\delta m^2\beta^2 \\ & -64m^2\alpha^2\delta\beta^2 + 96m^2\mathcal{N}_m(\alpha)\alpha^2\beta^2 - 32m^4\beta^2 \\ & -48\mathcal{N}_m(\alpha)\beta^2 + 128\alpha^2\beta^2 + 160\delta\beta^2 \\ & -168\mathcal{N}_m(\alpha)m^2\beta^2 - 192\mathcal{N}_m(\alpha)\alpha^2\beta^2 + 128\alpha^2\delta\beta^2 \\ & -64m^2\alpha^2\beta^2 + 96m^4\mathcal{N}_m(\alpha)\beta^2 - 20\mathcal{N}_m(\alpha)\delta\beta^2 \\ & -184m^2\delta - 32m^4\mathcal{N}_m(\alpha)\delta\beta^2 - 64\alpha^4\mathcal{N}_m(\alpha)\delta\beta^2 \\ & -16m^2\beta^2 - 184m^2 + 8\lambda^2 - 270\beta \\ & +48\alpha^4\mathcal{N}_m(\alpha)\lambda^2 + 160\beta^2 - 8m^4\lambda^4\mathcal{N}_m(\alpha) - 36\lambda^2m^2 \\ & +64m^4 - 8\lambda^4 + 64m^4\delta \\ & -16\alpha^4\lambda^4\mathcal{N}_m(\alpha) + 96m^2\mathcal{N}_m(\alpha)\alpha^2 - 16\lambda^4m^2\alpha^2 \\ & +216m^2\delta\beta - 32m^4\delta\beta^2 - 16m^2\delta\beta^2 \\ & +216m^2\beta + 32\alpha^4\mathcal{N}_m(\alpha) + 64m^4\mathcal{N}_m(\alpha) \\ & +18\delta\lambda^2\beta - 14\mathcal{N}_m(\alpha), \end{aligned} \quad (\text{D4})$$



$$\begin{aligned}
\mathcal{D} \equiv & 14 - 8\delta\lambda^2\alpha^2 - \mathcal{N}_m(\alpha)\lambda^2 + \lambda^4\mathcal{N}_m(\alpha) \\
& - 16m^4\lambda^2 - 2\lambda^4m^2\delta - 64m^2\lambda^2\alpha^2 \\
& + \delta\lambda^2 + 8m^4\lambda^4\delta - 16m^4\delta\lambda^2 \\
& - 2m^2\lambda^4 - 48\alpha^4\delta\lambda^2 + 16m^4\mathcal{N}_m(\alpha)\lambda^2 \\
& + 16m^4\mathcal{N}_m(\alpha)\delta\lambda^2\beta + 8\mathcal{N}_m(\alpha)\lambda^2\alpha^2 + 48\alpha^2 \\
& - 8\lambda^2\alpha^2 - 40m^2\mathcal{N}_m(\alpha) + 48\alpha^2\delta \\
& - 48\alpha^2\mathcal{N}_m(\alpha) + 2\lambda^4\mathcal{N}_m(\alpha)m^2 - \lambda^4\delta \\
& + 16\alpha^4\lambda^4\delta + 32m^2\mathcal{N}_m(\alpha)\delta\lambda^2\alpha^2\beta + 24m^2\lambda^4\delta\alpha^2 \\
& - 24m^2\lambda^4\mathcal{N}_m(\alpha)\alpha^2 - 32\alpha^4 - 64m^2\delta\lambda^2\alpha^2 \\
& + 16\lambda^4\alpha^4 - 96m^2\alpha^2 - 48\alpha^4\lambda^2 \\
& - 96m^2\alpha^2\delta - 32\alpha^4\delta + 8m^4\lambda^4 + 64m^2\mathcal{N}_m(\alpha)\lambda^2\alpha^2 \\
& - 32m^2\mathcal{N}_m(\alpha)\lambda^2\alpha^2\beta + 16\alpha^4\mathcal{N}_m(\alpha)\delta\lambda^2\beta \\
& + 30\mathcal{N}_m(\alpha)\beta - 128m^2\mathcal{N}_m(\alpha)\alpha^2\beta + 16\mathcal{N}_m(\alpha)\delta\alpha^2\beta \\
& + 32m^4\mathcal{N}_m(\alpha)\delta\beta + 32\alpha^4\mathcal{N}_m(\alpha)\delta\beta \\
& + 64m^2\mathcal{N}_m(\alpha)\delta\alpha^2\beta + 128m^2\alpha^2\delta\beta + 16\mathcal{N}_m(\alpha)\delta m^2\beta \\
& - 112\alpha^2\beta - 30\delta\beta + 96m^4\beta + 96\mathcal{N}_m(\alpha)m^2\beta \\
& + 112\mathcal{N}_m(\alpha)\alpha^2\beta - 112\alpha^2\delta\beta + 128m^2\alpha^2\beta \\
& - 96m^4\mathcal{N}_m(\alpha)\beta + 2\mathcal{N}_m(\alpha)\delta\beta + 2\lambda^2\beta \\
& + 32m^2\delta\lambda^2\alpha^2\beta + 16\delta\lambda^2\alpha^2\beta - 3\mathcal{N}_m(\alpha)\delta\lambda^2\beta \\
& + 32m^2\lambda^2\alpha^2\beta + 32\alpha^4\delta\lambda^2\beta - 8\mathcal{N}_m(\alpha)\lambda^2m^2\beta \\
& - 16\mathcal{N}_m(\alpha)\lambda^2\alpha^2\beta - 32\alpha^4\mathcal{N}_m(\alpha)\lambda^2\beta - 2\mathcal{N}_m(\alpha)\lambda^2\beta \\
& + 16\lambda^2\alpha^2\beta + 32\alpha^4\lambda^2\beta + 8\lambda^2m^2\beta + 14\delta + 32\alpha^4\beta \\
& + 32\alpha^4\delta\beta - 32\alpha^4\mathcal{N}_m(\alpha)\beta - 8\mathcal{N}_m(\alpha)\delta\alpha^2\beta\lambda^2 \\
& - 64m^2\mathcal{N}_m(\alpha)\delta\alpha^2\beta^2 - 8\mathcal{N}_m(\alpha)\delta m^2\beta\lambda^2 \\
& - 16\mathcal{N}_m(\alpha)\delta\alpha^2\beta^2 - 16\mathcal{N}_m(\alpha)\delta m^2\beta^2 - 32m^2\alpha^2\delta\beta^2 \\
& + 32m^2\mathcal{N}_m(\alpha)\alpha^2\beta^2 - 32m^4\beta^2 - 16\mathcal{N}_m(\alpha)\beta^2 \\
& + 64\alpha^2\beta^2 + 16\delta\beta^2 - 56\mathcal{N}_m(\alpha)m^2\beta^2 \\
& - 64\mathcal{N}_m(\alpha)\alpha^2\beta^2 + 64\alpha^2\delta\beta^2 - 32m^2\alpha^2\beta^2 \\
& + 32m^4\mathcal{N}_m(\alpha)\beta^2 - 2\mathcal{N}_m(\alpha)\delta\beta^2 + 40m^2\delta \\
& - 32m^4\mathcal{N}_m(\alpha)\delta\beta^2 - 32\alpha^4\mathcal{N}_m(\alpha)\delta\beta^2 + 56m^2\beta^2 \\
& + 40m^2 + \lambda^2 - 30\beta + 48\alpha^4\mathcal{N}_m(\alpha)\lambda^2 \\
& + 16\beta^2 - 8m^4\lambda^4\mathcal{N}_m(\alpha) - 64m^4 - \lambda^4 \\
& - 64m^4\delta - 16\alpha^4\lambda^4\mathcal{N}_m(\alpha) + 96m^2\mathcal{N}_m(\alpha)\alpha^2 \\
& + 24\lambda^4m^2\alpha^2 + 96m^4\delta\beta + 8m^2\delta\lambda^2\beta - 96m^2\delta\beta \\
& - 32m^4\delta\beta^2 + 56m^2\delta\beta^2 - 96m^2\beta + 32\alpha^4\mathcal{N}_m(\alpha) \\
& + 64m^4\mathcal{N}_m(\alpha) + 2\delta\lambda^2\beta - 14\mathcal{N}_m(\alpha) .
\end{aligned} \tag{D5}$$

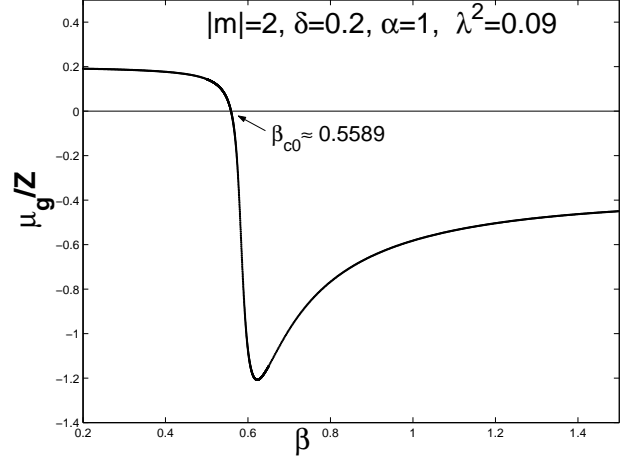


**Figure E1.** The phase relationship between the perturbation of gas density  $\mu_g$  and that of azimuthal magnetic field  $Z$ , with  $|m| = 2$ ,  $\delta = 0.2$ ,  $\alpha = 1$  and  $\lambda^2 = 0.09$ . This branch goes across the horizontal  $\beta$  axis consistent with formula (123).

parameters are exactly the same as those of Figure 23 and only the  $y_2$  branch is shown here) to support our statement in the main text. In Figure E1, it is clear that this  $y_2$  branch does indeed go across the horizontal  $\beta$  axis at about 0.5589 as expected from formula (123).

## APPENDIX E:

In section 4.3.2, we indicated that there exists a root  $\beta_{c0}$  for the  $y_2$  solution branch of the  $\mu_g/Z$ , and in the case of Figure 23, the value of this  $\beta_{c0}$  is about 0.5589 by formula (123). However, one might worry that from Figure 23 in which  $\beta$  ranges from 1 to 5, the trend of variation of  $y_2$  may not lead to such a  $\beta_{c0}$  where  $y_2$  vanishes. Here, we provide the  $\mu_g/Z$  versus  $\beta$  curve in which  $\beta$  ranges from 0.2 to 1.5 (all other